Ann. Geophysicae 18, 1503–1522 (2001) © EGS – Springer-Verlag 2001

Annales Geophysicae

Effect of the IMF B_y component on the ionospheric flow overhead at EISCAT: observations and theory

H. Khan, S. W. H. Cowley

Department of Physics and Astronomy, University of Leicester, University Road, Leicester LE1 7RH, UK

Received: 29 May 2000 / Revised: 11 October 2000 / Accepted: 11 October 2000

Abstract. We have analysed a database of ~300 h of tristatic ionospheric velocity measurements obtained overhead at Tromsø (66.3° magnetic latitude) by the EISCAT UHF radar system, for the presence of flow effects associated with the y-component of the IMF. Since it is already known that the flow depends upon IMF B_z, a least-squares multivariate analysis has been used to determine the flow dependence on both IMF B_y and B_z simultaneously. It is found that significant flow variations with IMF B_y occur, predominantly in the midnight sector (~2100–0300 MLT), but also pre-dusk (~1600–1700 MLT), which are directed eastward for IMF B_y positive and westward for IMF B_y negative. The flows are of magnitude 20–30 m s^{-1} nT^{-1} in the midnight sector, and smaller, 10–20 m s^{-1} nT^{-1}, pre-dusk, and are thus associated with significant changes of flow of order a few hundred m s^{-1} over the usual range of IMF B_y of about ± 5 nT. At other local times the IMF B_y-related perturbation flows are much smaller, less than ~5 m s^{-1} nT^{-1}, and consistent with zero within the uncertainty estimates. We have investigated whether these IMF B_y-dependent flows can be accounted for quantitatively by a theoretical model in which the equatorial flow in the inner magnetosphere is independent of IMF B_y, but where distortions of the magnetospheric magnetic field associated with a "penetrating" component of the IMF B_y field changes the mapping of the field to the ionosphere, and hence the ionospheric flow. We find that the principal flow perturbation produced by this effect is an east–west flow whose sense is determined by the north–south component of the unperturbed flow. Perturbations in the north–south flow are typically smaller by more than an order of magnitude, and generally negligible in terms of observations. Using equatorial flows which are determined from EISCAT data for zero IMF B_y, to which the corotation flow has been added, the theory predicts the presence of zonal perturbation flows which are generally directed eastward in the Northern Hemisphere for IMF B_y positive and westward for IMF B_y negative at all local times. However, although the day and night effects are therefore similar in principle, the model perturbation flows are much larger on the nightside than on the dayside, as observed, due to the day-night asymmetry in the unperturbed magnetospheric magnetic field. Overall, the model results are found to account well for the observed IMF B_y-related flow perturbations in the midnight sector, in terms of the sense and direction of the flow, the local time of their occurrence, as well as the magnitude of the flows (provided the magnetic model employed is not too distorted from dipolar form). At other local times the model predicts much smaller IMF B_y-related flow perturbations, and thus does not account for the effects observed in the pre-dusk sector.

Key words: Magnetospheric physics (magnetosphere–ionosphere interactions) – Ionosphere (plasma convection; auroral ionosphere)

1 Introduction

Observations by polar-orbiting spacecraft and ground-based radars have amply demonstrated that the flow in the high-latitude ionosphere is strongly modulated by the direction of the interplanetary magnetic field (IMF) (e.g. Reiff and Burch, 1985; Heppner and Maynard, 1987; Rich and Hairston, 1994; Weimer, 1995; Ruohoniemi and Greenwald, 1996). The form of the convection, whether two or more cells, together with their overall size and strength, are determined principally by the IMF B_z component. When IMF B_z is negative the flow is twin-celled, with antisunward flow over the polar cap and return sunward flow in the auroral zones. For positive IMF B_z these flows weaken, contract poleward, and cells with a "reversed" sense of flow may appear within the polar cap. These effects are controlled principally by the location and rates of magnetic

Correspondence to: H. Khan
e-mail: hina.khan@ion.le.ac.uk

reconnection between the magnetosheath and magnetospheric fields at the magnetopause boundary, and consequent activity in the tail (Dungey, 1961; Crooker, 1979; Lockwood, 1995).

The IMF B_y component also plays a significant role, however, and is associated with a set of dawn-dusk asymmetries in the ionospheric flow pattern, with primary effects occurring on open field lines within the polar cap. These asymmetries reverse in sense with IMF B_y, and are oppositely-directed in the Northern and Southern Hemispheres. Specifically, the flow of newly opened field lines in the dayside cusp is directed westward in the Northern Hemisphere when IMF B_y is positive, and eastward when it is negative, and vice-versa in the Southern Hemisphere (e.g. Galperin *et al.*, 1978; Heelis, 1979). These flows are directly associated with the Svalgaard-Mansurov effect in ground magnetic data at cusp latitudes, and related signatures in the cusp field-aligned current system (e.g. Friis-Christensen and Wilhjelm, 1975; Iijima *et al.*, 1978; McDiarmid *et al.*, 1978). The flows are believed to be due to the effect of the magnetic tension force acting on newly reconnected flux tubes in the presence of IMF B_y (Jørgensen *et al.*, 1972). For IMF B_y positive, for example, open tubes are pulled westward in the Northern Hemisphere and added preferentially to the dawn side of the northern tail lobe, while simultaneously being pulled eastward in the Southern Hemisphere and added preferentially to the dusk side of the southern tail lobe, and vice versa for IMF B_y negative. The antisunward flow over the polar cap is thus correspondingly asymmetric, with stronger flows on the dawn side in the Northern Hemisphere for IMF B_y positive, and simultaneously on the dusk side in the Southern Hemisphere, and vice versa for IMF B_y negative (Heppner, 1972). The overall effect on open field lines is thus to add a westward zonal circulation to the Northern Hemisphere flow when IMF B_y is positive, and an eastward zonal circulation when IMF B_y is negative, and vice versa in the Southern Hemisphere.

Other IMF B_y-related effects have also been observed which imply the existence of flow asymmetries on closed field lines as well. Newell *et al.* (1989) have reported that the local time of the dayside cusp moves in response to IMF B_y, to the postnoon hours in the Northern Hemisphere for IMF B_y positive, and to the prenoon hours for IMF B_y negative, and vice versa in the Southern Hemisphere. This implies that closed field lines have a preferential eastward and poleward flow into the post-noon cusp in the Northern Hemisphere for IMF B_y positive, and a preferential westward and poleward flow into the pre-noon cusp for IMF B_y negative, and vice versa in the Southern Hemisphere. Similarly, Rodger *et al.* (1984) and Heppner and Maynard (1987) report that on the nightside, the Harang discontinuity occurs at earlier local times in the Northern Hemisphere for IMF B_y positive, and later for IMF B_y negative, and vice versa in the Southern Hemisphere. Since the Harang discontinuity marks the point where the nightside zonal flow reverses from west to east with increasing local time, this effect can also be viewed as being due to the presence of additional eastward flows in the Northern Hemisphere for IMF B_y positive, and westward flows for IMF B_y negative, and vice versa in the Southern Hemisphere. Finally, many studies have shown that the polar cap as a whole is shifted towards dawn in the Northern Hemisphere for IMF B_y positive, and towards dusk for IMF B_y negative, and vice versa in the Southern Hemisphere (e.g. Holzworth and Meng, 1984; Heppner and Maynard, 1987). This implies that in the Northern Hemisphere for IMF B_y positive the return sunward flow in the dusk auroral zone is spread over a greater latitude range than on average and is hence weakened, while in the dawn auroral zone it is concentrated over a smaller latitude range and is hence strengthened, with opposite effects occurring simultaneously in the Southern Hemisphere. These perturbations are again equivalent to adding eastward flows to the sunward return flows at dawn and dusk in the Northern Hemisphere for IMF B_y positive, and westward flows for IMF B_y negative, and vice versa in the Southern Hemisphere. Taken together, these effects discussed associated with the dayside cusp, the Harang discontinuity, and the dawn-dusk shift of the polar cap, all imply the existence of an eastward zonal flow on closed field lines in the Northern Hemisphere for IMF B_y positive, and a westward zonal flow for IMF B_y negative, and vice versa in the Southern Hemisphere. This sense of flow is thus the opposite to that which occurs simultaneously at higher latitudes on open field lines in the corresponding polar caps. Both are implicit in the recent statistical models derived from spacecraft and radar data cited, for example, those of Weimer (1995) and Ruohoniemi and Greenwald (1996).

While the presence of oppositely directed zonal flows and consequent opposite asymmetries in the northern and southern hemispheres presents no conceptual difficulties on open field lines in the polar caps, the existence of related effects on closed field lines as well raises issues of the apparent lack of inter-hemispheric conjugacy. In general, the resolution of these issues requires that the magnetic field lines in the closed region of the magnetosphere undergo IMF B_y-dependent distortions such that conjugacy is in fact maintained. For example, it is inevitable that the closed field lines that are moving into the post-noon cusp in the Northern Hemisphere when IMF B_y is positive are magnetically connected to the closed field lines that are simultaneously moving into the pre-noon cusp in the Southern Hemisphere. Similarly, the last closed field lines mapping to the open-closed field line boundaries at dawn and dusk at differing magnetic latitudes in the two hemispheres must also be magnetically connected, as must the field lines mapping to the northern and southern Harang discontinuities. It was shown by Cowley (1981) that the field distortions required to maintain conjugacy in these circumstances can be qualitatively accounted for by the presence of a B_y field in the region of closed field lines which has the same sense as the interplanetary B_y. That is, the y-component of the interplanetary field must at least partially "penetrate" into the magnetosphere, as expected on basic theoretical grounds in a magnetically "open" system. Figure 1, taken from Cowley *et al.* (1991), shows the field

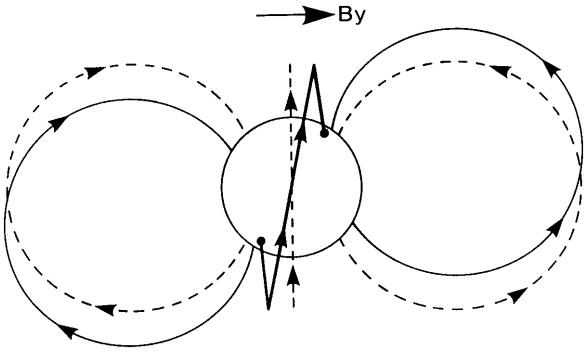

Fig. 1. Sketch showing the distortions of the Earth's closed field lines produced by adding a uniform field in the $+y$-direction (*left* to *right*), viewed from the direction of the Sun. The *solid lines* are the distorted field lines, and the *dashed lines* the corresponding undistorted field lines (From Cowley *et al*., 1991.)

distortions that take place when a field in the $+y$-direction (left to right) is added to a dipolar field. The dashed lines show the undistorted dipolar field lines, while the solid lines show the distorted field lines. At noon and midnight the field becomes tilted out of meridian planes to join dusk-side points in the Northern Hemisphere to dawn-side points in the Southern Hemisphere, as required to maintain conjugacy of the flow into the cusp and in the Harang region. Simultaneously, the field lines become displaced in latitude at dawn and dusk consistent with the observed dawn-dusk displacements of the polar cap. The consequent differential zonal flows between Northern and Southern Hemispheres then act to tilt the field out of the magnetic meridians between nightside and dayside orientations as the field lines propagate in local time. Subsequently, it has been shown that such IMF B_y-related perturbation fields do indeed exist in the region of closed field lines. At geostationary orbit, for example, the penetrating field is found typically to be a significant fraction of the simultaneous IMF B_y field (Cowley and Hughes, 1983; Nagai, 1987; Wing *et al*., 1995).

We investigate a database of ~300 h of EISCAT observations of the F-region ionospheric flow overhead at Tromsø, located in the closed-field line auroral zone region at 66.3° magnetic latitude (nominally near-conjugate to geostationary orbit), to quantitatively determine the dependence of the flow on IMF B_y, and how this varies with magnetic local time (MLT). We have then compared these observations with those expected theoretically on the basis of the field-distortion hypothesis outlined to determine the degree to which the observed flow perturbations can be accounted for quantitatively on this basis.

2 Data sets and analysis procedure

The measurements of ionospheric flow employed in this study were obtained by the tristatic EISCAT UHF incoherent scatter radar system using the CP-1-K common programme experiment, which has been run typically on several days each year since 1993. In this experiment the radar beam is pointed along the magnetic field line at Tromsø (Norway), approximately southward at an elevation angle of 77.5°, while remote site receivers at Kiruna (Sweden) and Sodankylä (Finland) are pointed at a fixed intersection with the transmitted beam at an F-region altitude of 278 km. Continuous tristatic measurements of the plasma flow at a single point essentially overhead at Tromsø are thereby obtained. The measurement point corresponds to a magnetic latitude of 66.3°, or an L-value of 6.2 R_E, nominally close to geostationary orbit (at an equatorial radial distance of 6.6 R_E) in the region of closed field lines. The radar data are integrated over 2 min intervals, thus setting the temporal resolution of the velocity measurements used in this study.

To determine the dependence of the flow on IMF B_y, the radar data have been analysed by means of a multivariate analysis technique with concurrent IMF measurements made by the IMP-8 spacecraft. This spacecraft moves in a near-circular orbit at 35 R_E, and provides vector IMF data at 15 s resolution, and solar wind plasma data with a resolution between 60 and 300 s. The latter data are employed to estimate the propagation delay of the IMF between the spacecraft and first effects in the polar ionosphere. This estimate includes the propagation delay (1) from the spacecraft to the subsolar bow shock taking account of the "phase front" orientation of variations in the IMF, (2) the propagation across the subsolar magnetosheath from bow shock to magnetopause, whose positions are determined from empirical models, and (3) a 2 min Alfvénic propagation along open field lines into the polar ionosphere. Full details may be found in Khan and Cowley (1999), where essentially the same radar and IMF data set was used to investigate flow modulations associated with IMF B_z (though the data employed here has been somewhat augmented on the nightside to improve statistics). Once the propagation delay for a particular interval has been determined (typically lying in the range 5–15 min with an estimated uncertainty of ± 2 min), this has been removed prior to averaging the 15 s IMF data over the "same" 2 min intervals as the radar data. These joint 2 min-averaged "simultaneous" radar-spacecraft data sets form the basis of the multivariate analysis presented here. Overall, about 300 h of simultaneous data are employed, obtained during 1993–97. The data span all local times, though the hemisphere centred on dusk is favoured relative to the hemisphere centred on dawn. Typically ~8 radar experiment-days contribute data at each local time in the dawn hemisphere, and ~13 experiment-days in the dusk hemisphere (see Khan and Cowley, 1999, for further details).

To investigate the variation of IMF B_y-associated effects with MLT, we have divided the ionospheric flow data into overlapping 2 h intervals of MLT, in steps of 1 h of MLT, and we consider the behaviour of the field-perpendicular flow components directed towards magnetic east, v_E, and magnetic north, v_N. Since the flow is known to depend strongly upon IMF B_z (e.g. Khan and Cowley, 1999), in addition to any possible IMF B_y effects, we have performed a least-squares multivariate fit to the data, in which the flow dependencies on IMF B_z

and B_y are obtained simultaneously. That is, we have fit the radar velocity component data to the linear function

$$v' = v_o + g_y B_y + g_z \mathscr{V}^2 B_S \ . \quad (1)$$

Here the IMF B_z dependence is parameterised in terms of the "half-wave rectifier" function $\mathscr{V}^2 B_S$ (as in Khan and Cowley, 1999), where $\mathscr{V}$ is the speed of the solar wind normalised to 500 km s^{-1} [i.e. $\mathscr{V} = (V_{SW}(\text{km s}^{-1})/500)$], and $B_S = B_z$ when B_z is negative while $B_S = 0$ when B_z is positive. Previous studies have indicated that this function generally gives the highest correlations with ionospheric flows (e.g. Etemadi *et al.*, 1988). The output parameters of greatest interest for this study are the gradient coefficients g_y which describe the dependency of the flow on IMF B_y, but we will also display the values of v_o and g_z as well, for purposes of comparison with the corresponding results derived previously by Khan and Cowley (1999). The coefficients are determined for a given subset of the data by finding the values which minimise the normalised fit parameter f given by

$$f = \sum_{i=1}^{n} \left(v_i - v_i'\right)^2 \Big/ \sum_{i=1}^{n} v_i^2 \ , \quad (2)$$

applicable to either eastward or northward flow components, where the v_i are the velocity component data values, and the v_i' are given by Eq. (1). They are obtained by equating the partial differentials of f with respect to the coefficients to zero, yielding three simultaneous linear equations which can be solved for the coefficients. For each subset of the flow data, corresponding to a given MLT sector, this procedure is carried out for a range of delay times between the flow measurements and the corresponding interplanetary parameters. A global minimum in f for that data set should then occur at the time corresponding to the response delay of the flow in that MLT sector to the first arrival of IMF effects in the ionosphere. Our goal is thus to determine the coefficients, principally the g_y values, which correspond to the delay time giving the best fit of Eq. (1) to the data (i.e. the smallest value of f). The delay times determined will also be displayed for comparison with the corresponding results of Khan and Cowley (1999), derived using cross-correlation between the ionospheric velocity components and the above "half-wave rectifier" function.

The top panels of Fig. 2 show typical examples of the normalised fit parameter f determined for each of the flow components, v_E (left) and v_N (right), shown versus delay time over an interval of -10 to $+60$ min, with a resolution of 2 min (the resolution of the data). For positive delays the interplanetary medium leads the ionosphere, while for negative delays the ionosphere (unphysically) leads the interplanetary medium. Figure 2a shows results for the dayside local time sector 1000–1200 MLT. A clear minimum in the fit parameter is observed in the results for both v_E and v_N at a delay of 2 min. This corresponds exactly to the delay previously determined from the maximum in the cross-correlation function between these flow components and $\mathscr{V}^2 B_S$ by Khan and Cowley (1999). The lower panels show scatter plots of the velocity components versus IMF B_y at that delay time, where the IMF B_z effect has been "removed" from the data using Eq. (1). That is, we plot $v_i - g_z \mathscr{V}^2 B_S$ for the g_z value corresponding to that flow component and delay time, thus removing the systematic variations with IMF B_z, and leaving only the possible IMF B_y effects, plus scatter due to other flow effects not accounted for in the analysis (e.g. non-linear responses, ULF waves, substorms, etc.). These values of g_z were found to be 17.7 and -12.3 m s^{-1} nT^{-1} for v_E and v_N, respectively, in this case. The central solid lines in the scatter plot then show the least-squares linear fit between this "corrected" velocity data and IMF B_y, the slope of which is just the value of g_y in Eq. (1). In this case, however, the value is found to be 1.2 ± 1.7 m s^{-1} nT^{-1} for v_E, and -2.0 ± 1.1 m s^{-1} nT^{-1} for v_N, such that both are very small, and essentially consistent with zero within the standard errors of the slope of the least-squares fit. The flanking solid lines in the scatter plot show these uncertainties in the slope, where the lines have been drawn through the point representing the average of the velocity component and IMF B_y measurements (through which point the best fit line also always passes). Such null results are found to be typical of those obtained in the dawn and dayside sectors (0400–1500 MLT). Thus although in principle IMF B_y-related flows may in general be expected at these local times, as indicated in the introduction, they are clearly not of significant amplitude at EISCAT latitudes.

In Fig. 2b, however, results for the nightside sector are shown, for the interval 0000–0200 MLT. Here the fit parameter f for v_E shows a broad but well-defined minimum, between delay times of ~14 to ~40 min, with a global minimum at 34 min (again consistent with the results of Khan and Cowley, 1999). The scatter plot for v_E at this delay shown beneath (with an IMF B_z effect associated a g_z value of -41.3 m s^{-1} nT^{-1} removed), now indicates a strong variation of the flow with IMF B_y. This result is found to be insensitive to the value taken for the delay time within the minimum. The mean eastward flow is near to zero for IMF $B_y \approx -5$ nT, but increases to ~600 m s^{-1} for IMF $B_y \approx +5$ nT. The gradient of the least-squares best fit line is correspondingly found to be $g_y = 65.7 \pm 7.3$ m s^{-1} nT^{-1}, a significant value clearly not consistent with zero within the uncertainty limits. The sense of the change in the flow, with increasing eastward flow for increasing IMF B_y, is in conformity with the discussion in the introduction. Although the magnitude of this effect is the largest of those found in the data set examined here (being about twice the average midnight-sector value), such positive gradients in v_E are found to be typical of the data in the dusk (~1600–1700 MLT) and midnight (2100–0300 MLT) sectors, as will be shown later. Turning now to the data for v_N shown on the right side of Fig. 2b, it can first be seen that the fit parameter f is near unity, and shows only weak variations with delay time and no significant minimum for positive delays. This is indicative of only weak control of this flow component in this MLT sector by the IMF, as also found by Khan and Cowley (1999). In this case, we therefore show the scatter plot for v_N at the same 34 min lag as for v_E (with a weak IMF B_z effect associated with a g_z value of 6.4 m s^{-1} nT^{-1}

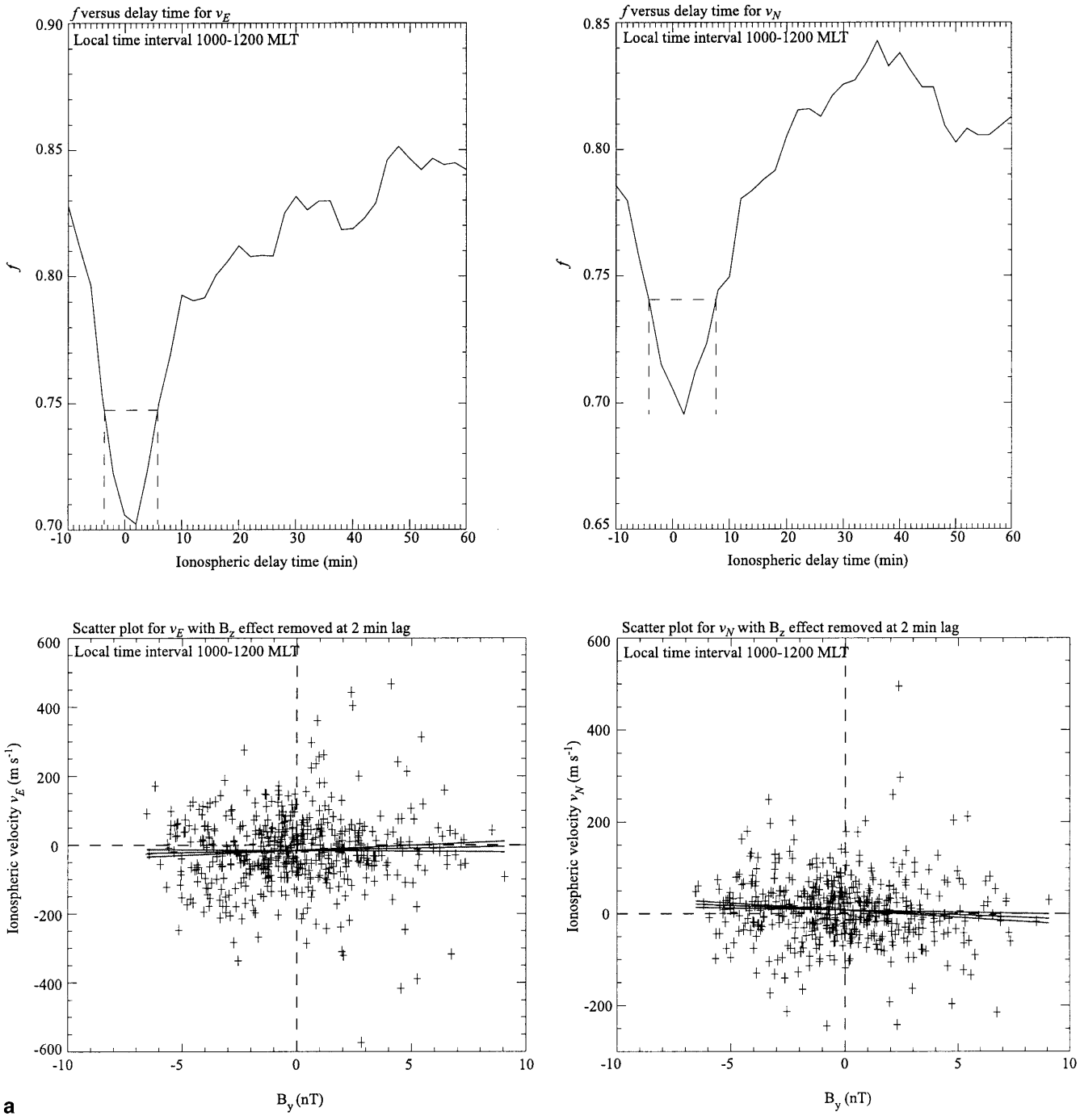

Fig. 2a.

removed). The gradient of the best fit line with respect to IMF B_y is found to be 8.8 $\pm$ 4.2 m s^{-1} nT^{-1}, as shown, associated with only weak variations of the north–south flow over the usual range of IMF B_y. Weak gradients in v_N, near the limits of uncertainty, are found to be typical of the dusk and midnight sectors.

3 Observational results

Having introduced the analysis procedures and initial results in the previous section, we now turn to the overall results. Although not a principal concern of the present work, in Fig. 3 we first show the results for the delay time between the interplanetary parameters and the flow response obtained from the minima in the fit function f. These demonstrate that the delays are essentially the same as those determined from the cross-correlation study between the flow components and $v^2 B_S$ by Khan and Cowley (1999). Figure 3a shows the delay time versus MLT (centred at midnight) obtained from the v_E data, plotted as solid circles. The error bars have been determined by the method illustrated by the dashed lines in the upper panels of

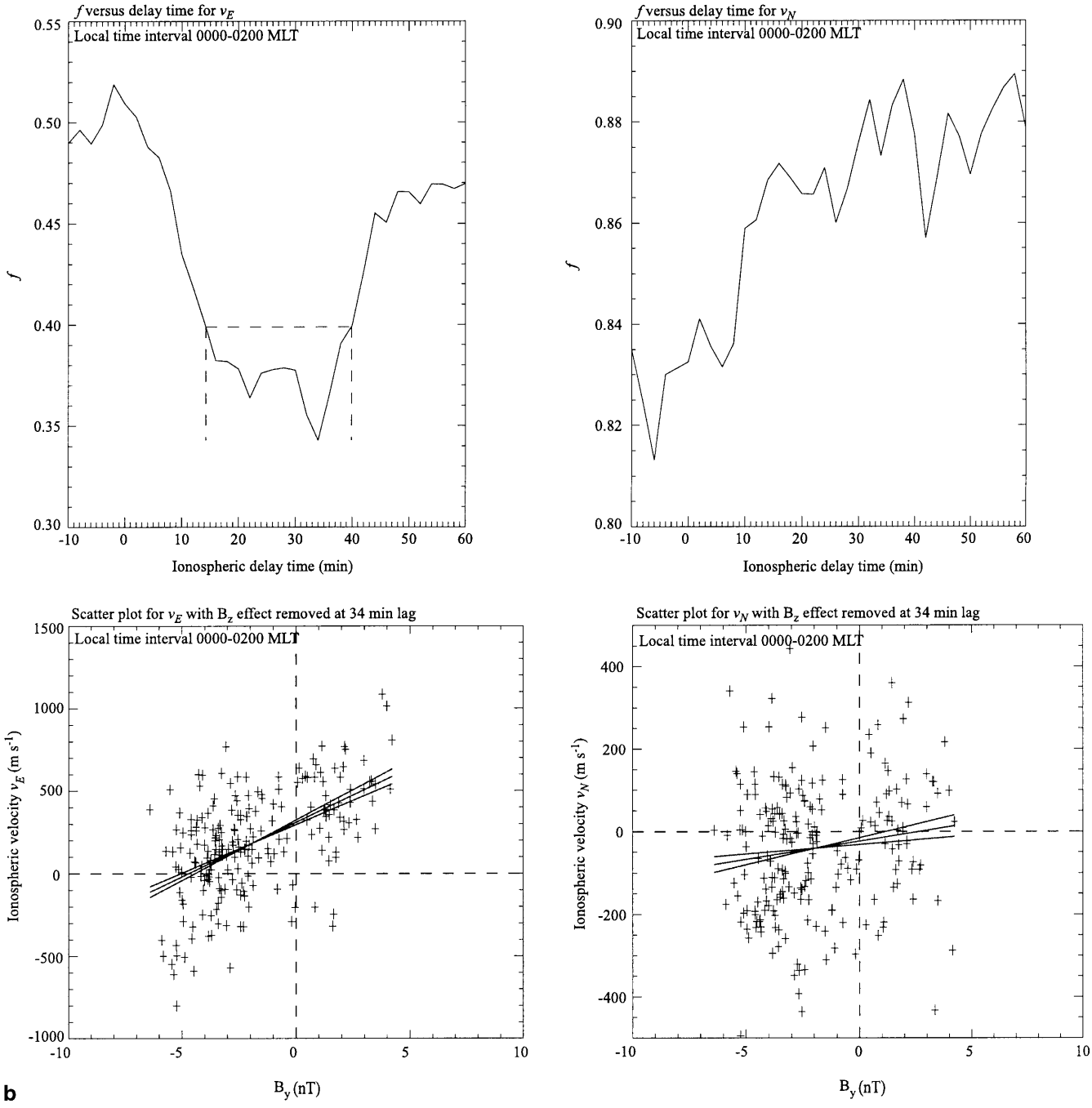

Fig. 2a, b. Normalised fit parameter f of the multivariate analysis given by Eq. (2) versus delay time, and corresponding scatter plots of velocity versus IMF B_y, for **a** 1000–1200 MLT, and **b** 0000–0200 MLT. In both cases the *left-hand plots* are for v_E, and the *right-hand plots* are for v_N. The *upper panels* show the fit parameter f versus delay time in the range −10 to +60 min, where the interplanetary parameters lead the ionosphere for positive lags. The *scatter plots beneath* correspond to the delay time for which the value of f is smallest, in the cases where the latter has a well-defined minimum. The estimated uncertainty in the delay time is indicated by the *dashed lines* in the *upper panels*. We first identify the distinct "slot" associated with the minimum in f, and then take the width of the "slot" half-way between its "top" and the minimum f value, as indicated by the *horizontal dashed line*. The *scatter plots* show the corresponding velocity component versus IMF B_y, where the variation with IMF B_z has been removed from the velocity data by use of the g_z coefficient obtained from the fit. The *central solid line* is the least-squares fit to this data, while the *flanking lines* indicate the uncertainty in the slope. All lines pass through the point corresponding to the mean velocity component value and the mean IMF B_y value of the data set shown

Fig. 2. We first identify the "slot" in the f values associated with the minimum, and then take the width of the "slot" half-way between its "top" and the minimum f value. It can be seen from Fig. 2 that this gives a reasonable estimate of the uncertainties in the position of the minimum. The delay times are typically

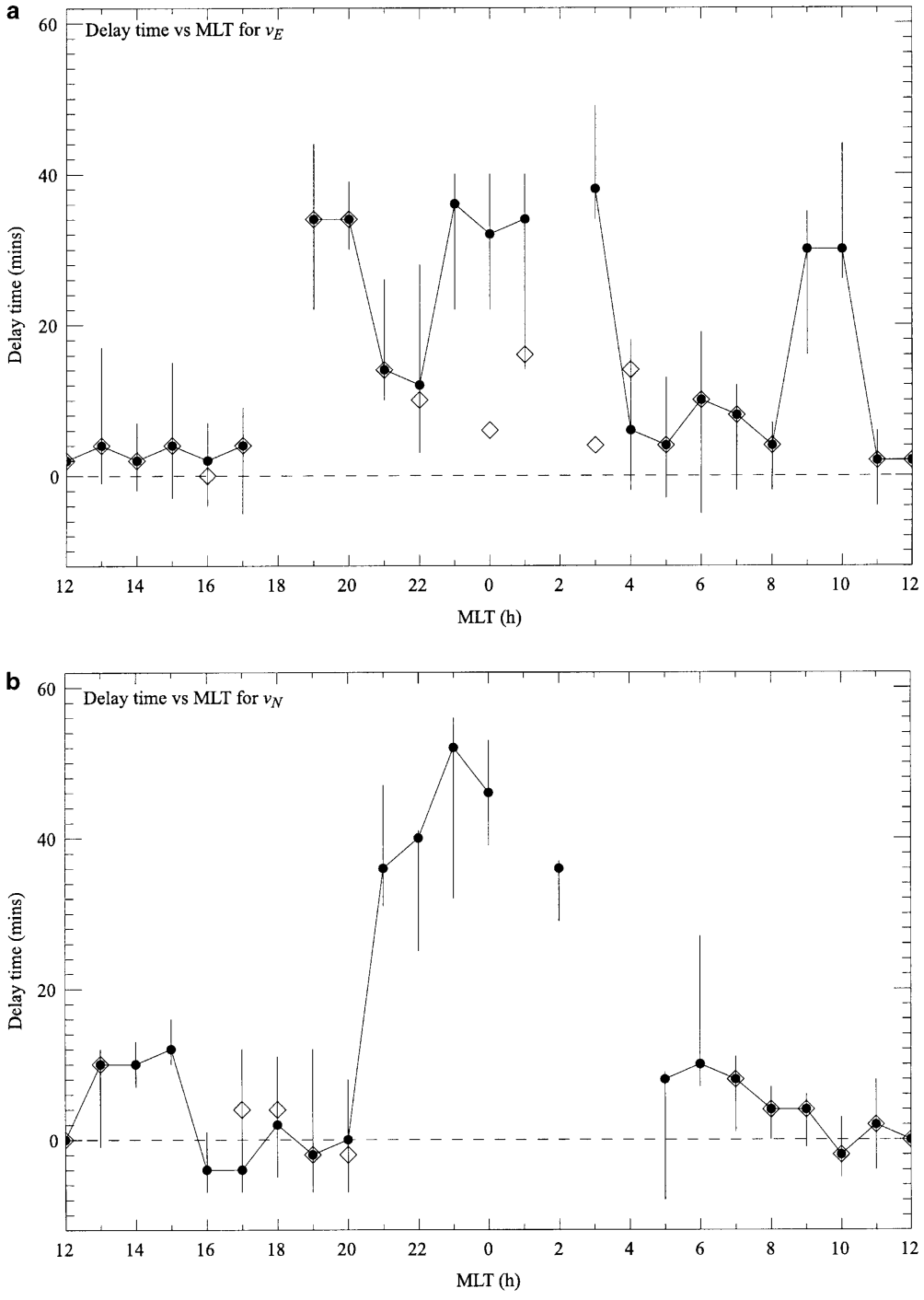

Fig. 3a, b. Flow response delay times versus MLT (centred on midnight) obtained from the minimum in the multivariate fit parameter f for **a** v_E, and **b** v_N, shown by the *solid circles* joined by *straight lines*. The error bars have been determined as indicated in Fig. 2. The *open diamonds* show the values determined by Khan and Cowley (1999) from a single-parameter cross-correlation analysis of the corresponding flow components with $\mathscr{V}^{-2}B_S$

short on the dayside, ~2 to ~8 min, and longer on the nightside, ~10 to ~35 min, consistent with the cross-correlation results of Khan and Cowley (1999). The values determined in the latter study are shown by diamonds for purposes of comparison, and with few exceptions are consistent with the results of the present study, within the uncertainty limits. Similar comments apply to the delay times determined from the v_N data, shown in the same format in Fig. 3b, which also show short delay times on the dayside, longer in the midnight sector, and agreement with the prior results of Khan and Cowley (1999).

The principal observational results of our study are shown in Fig. 4, where the coefficients v_o, g_y, and g_z, defined by Eq. (1), are plotted versus MLT (centred at midnight) which correspond to the fits obtained at the delay times shown in Fig. 3. Results for v_E are shown in Fig. 4a. At the top of the plot the value of v_o is shown, corresponding to the flow when B_S and B_y are both zero (basically the mean "background" flow for northward IMF). The flows are directed westward from pre-noon through dusk to pre-midnight, and eastward from pre-midnight through dawn to pre-noon, consistent with a somewhat rotated relatively weak normal twin-cell flow

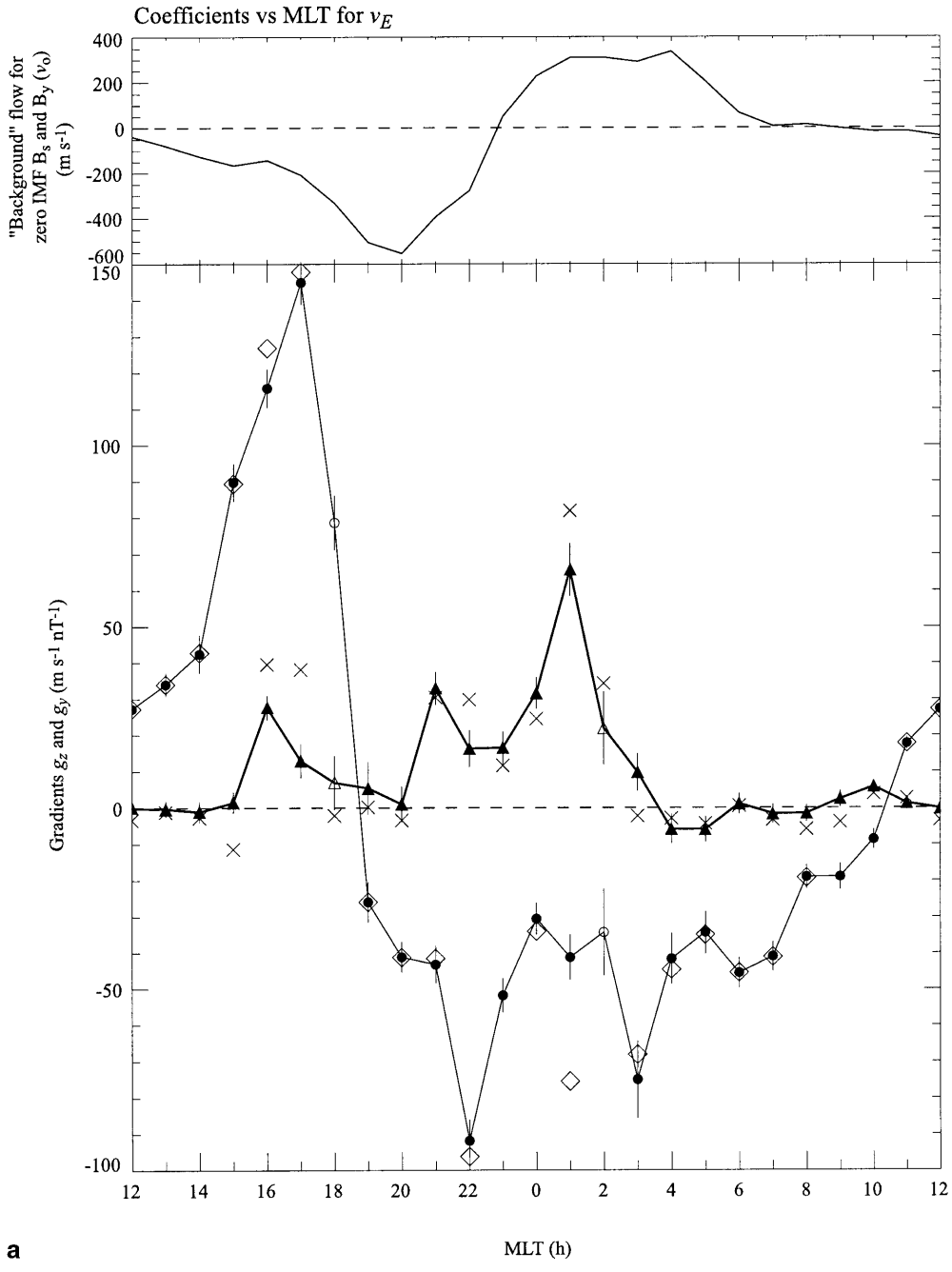

a

Fig. 4a.

pattern. The gradients g_z and g_y with respect to $v^2 B_S$ and B_y, respectively, are shown beneath. The values of g_z are shown by the solid circles joined by a thin solid line. Where no clear minimum in the fit parameter f was evident, the delay time corresponding to the minimum in the fit parameter for the other velocity component was used. The coefficients calculated in this manner are shown by open symbols. For v_E this applies only to two cases, centred at 0200 and 1800 MLT, where it is nevertheless clear that the results follow the overall trends very well. It can be seen that the values of g_z are positive from pre-noon to dusk, and negative from dusk through midnight and dawn to pre-noon. Since $v^2 B_S$ takes only negative values, this corresponds to increasing westward flows with negative IMF B_z in the former sector, and increasing eastward flows in the latter. Comparison with the upper panel shows that this simply corresponds to the expected enhancement of the twin-cell flow pattern for negative IMF B_z. The only exception to this statement occurs in the post-dusk sector, where v_o and g_z are both negative, implying a westward flow for positive IMF B_z which weakens and reverses towards eastward as IMF B_z becomes increasingly negative. This effect corresponds to the expected westward motion of the Harang discontinuity at a given auroral latitude as the flow pattern expands, as found previously by Khan and Cowley (1999). The corresponding gradient values obtained in the latter study are shown by the open diamonds in Fig. 4a, and clearly agree with the present

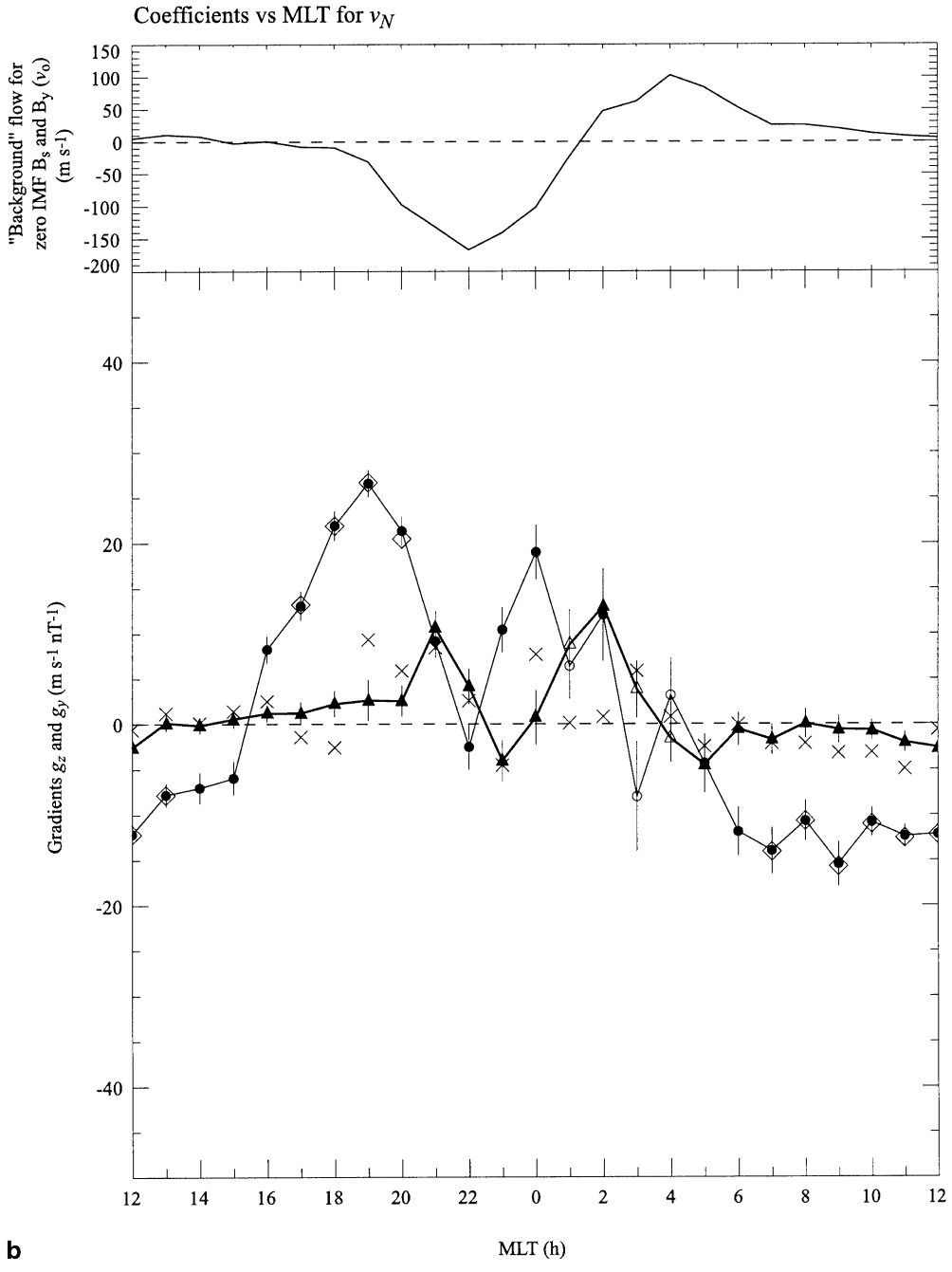

Fig. 4a, b. Coefficients of the multivariate analysis of the dependence of the flow components on interplanetary $\mathscr{V}^2 B_S$ and B_y, for **a** v_E, and **b** v_N, plotted versus MLT (centred on midnight). The coefficients are as defined in Eq. (1). The *upper panel* shows v_o, the "background" flow when B_y and B_S are both zero (essentially the mean flow for northward IMF). *Beneath* this we show the flow gradients g_z (*solid circles* joined by a *thin line*) and g_y (*solid triangles* joined by a *thick line*), determined at the delay times which give the minimum *f* value, as shown in Fig. 3. In those few cases where there is no clear minimum in *f*, we have used the delay time determined from the other flow component. These values are shown by the *open symbols* of similar type. The results of straightforward single-variable cross-correlation analyses between the flow component and the corresponding interplanetary parameters are also shown in the *lower panel*. Results for $\mathscr{V}^2 B_S$ are shown by *diamonds*, determined at the delay times of the peaks in the corresponding cross-correlation functions, taken from Khan and Cowley (1999). Results for IMF B_y are shown by *crosses*, determined at a fixed delay time of 20 min

results very well. Typical gradients are $g_z \approx 50$ m s^{-1} nT^{-1}, corresponding to a substantial change in the flow of $\sim$250 m s^{-1} for $\mathscr{V}^2 B_S \approx -5$ nT, a not untypical value.

The main new results of our study, however, are the g_y values shown by the triangles joined by a thick solid line in the lower panel of Fig. 4a, which give the gradient of the flow component relative to IMF B_y. In agreement with the results shown in the previous section, it can be seen that the values are small, essentially consistent with zero, in the post-midnight, dawn, and dayside sector, from 0300–1500 MLT. However, the values are consistently positive, and inconsistent with zero within the uncertainty limits (determined as the standard error of the least-squares fit gradient), both in the pre-dusk sector, 1600–1700 MLT, and in the midnight sector, 2100–0300 MLT. A positive value of g_y implies increasing eastward flows with increasing IMF B_y, consistent with the theoretical discussion in the introduction. The average value of g_y over the interval 1600–0200 MLT is 21.7 $\pm$ 1.6 m s^{-1} nT^{-1}, increasing to 30.8 $\pm$ 3.1 m s^{-1} nT^{-1} if we restrict attention to the midnight sector, 2100–0200 MLT, where the effect is largest and most consistent. Although these values are rather smaller than the corresponding gradients associated with IMF B_z (i.e. the g_z values), they are nevertheless associated with significant changes in the flow, as already evident in Fig. 2b. As indicated in the latter figure, the typical range of IMF B_y values is roughly $\pm$5 nT, thus giving changes in the east–west flow

of $\sim$300 m s^{-1} over this range of IMF B_y, if $g_y \approx 30$ m s^{-1} nT^{-1}. Such changes are not insignificant relative to typical values of the flow, as is evident from the v_o values shown in the top panel of the figure.

In order to investigate the robustness of the results concerning the dependence of the flow on IMF B_y, we have also analysed our data set using two other methods. First, we have simply performed a single-parameter cross-correlation analysis between the flow components and IMF B_y, analogous to the analysis between the flow components and $\mathscr{V}^2 B_S$ presented previously by Khan and Cowley (1999). The results show that, unlike the case of $\mathscr{V}^2 B_S$, the cross-correlation coefficient with respect to IMF B_y alone does not depend strongly on the delay time, over positive delays typically of several tens of minutes. This fact we attribute principally to the greater persistence of the value of IMF B_y in the interplanetary medium than IMF B_z (as verified by auto-correlation analysis of the IMF data used here). In this situation the gradients of the flow component with respect to IMF B_y have simply been determined by least-squares fits at a fixed typical delay time of 20 min (the results are insensitive to the exact choice). The gradients so determined are shown by crosses in Fig. 4a, and are clearly quite close to the values determined here using the multivariate fit. Second, at an even cruder level, the data in each MLT sector has been divided into two groups, for IMF B_y positive and negative (at various fixed delay times over an interval of a few tens of minutes), and each group averaged to find the mean flow component and the mean IMF B_y. A gradient has then been determined from the differences between these averaged values. Again the results (not shown) indicate the same features as those shown in Fig. 4a. We are therefore convinced that the IMF B_y-related effects indicated in Fig. 4a are robust features of the data set employed here.

Results for v_N are shown in Fig. 4b in the same format as Fig. 4a. The value of v_o shown in the upper panel is negative from pre-dusk through to the post-midnight sector, and positive from post-midnight to post-noon, again reflecting a somewhat rotated twin-cell flow pattern. The gradient g_z of the flow with respect to $\mathscr{V}^2 B_S$ shown by the solid and open circles (joined by a thin line) is essentially in antiphase with this variation, again indicative of a growth in the magnitude of these flows with negative IMF B_z. The diamonds are the corresponding gradients determined from the cross-correlation analysis of Khan and Cowley (1999), with which the present values are seen to be in excellent agreement. The triangles joined by the thick line show the gradient g_y with respect to IMF B_y. These tend to be small, rather scattered on the nightside, and in only two or three cases are the values seemingly inconsistent with zero. The crosses again show the gradients determined from a simple cross-correlation between v_N and IMF B_y, at a fixed lag of 20 min, and indicate a similar behaviour. Overall we conclude that there is no clear significant dependency of the north–south component of the flow on IMF B_y in this data set.

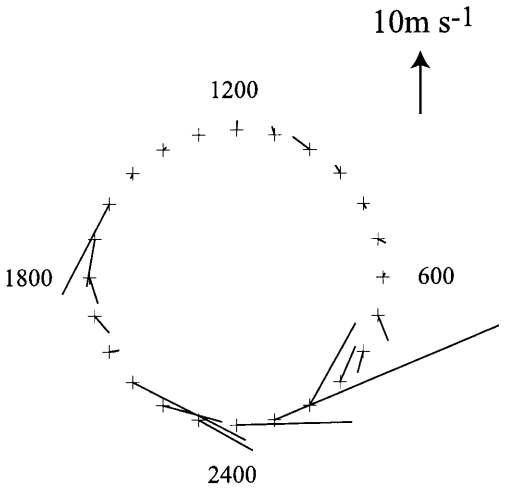

Fig. 5. Perturbation flow vectors for a +1 nT IMF B_y component in the interplanetary medium, relative to zero IMF B_y, obtained from the values of the gradient coefficients g_y for v_E and v_N in Fig. 4, plotted versus MLT in a polar format with noon at the *top* and dusk to the *left*. For a −1 nT IMF B_y component, the perturbation flow is reversed in direction

A summary of our results on the flow dependence on IMF B_y is shown in Fig. 5, where the gradient coefficients g_y for v_E and v_N are displayed as vectors on a polar plot versus MLT, with noon at the top and dusk to the left. This plot thus shows the direction and magnitude of the perturbation flow vector for a 1 nT positive IMF B_y field in the interplanetary medium, relative to zero IMF B_y. For a 1 nT negative IMF B_y field the perturbation flow vectors would be reversed in direction. This plot emphasises the fact that the perturbation flow vectors are directed principally east–west, with much smaller and variable north–south components, and are eastward in sense for IMF B_y positive. Principal effects are confined to the region three hours on either side of midnight, where the perturbation vectors are of magnitude $\sim$20–30 m s^{-1} nT^{-1}, though there is also a weaker effect of a similar nature in the dusk sector. Other than this, there is essentially no response of the flow to IMF B_y on the dayside at EISCAT latitudes.

4 Theoretical model

In this and the following section we investigate the degree to which the "field distortion" picture of the origin of IMF B_y-dependent flow perturbations on closed field lines, outlined in the introduction, can account quantitatively for the observed perturbation flows determined. That is, we assume that the flow in the equatorial plane of the magnetosphere is fixed, and examine the changes in ionospheric flow which result from the altered field mappings arising from a "penetrating" IMF B_y field. In this section the theoretical procedures we have adopted are described, while in the next the results will be described and compared with the above observations.

Our first task is to determine the unvarying flow in the equatorial plane which is to be mapped from the equator into the ionosphere along the distorted field

lines. This equatorial flow has been obtained from the EISCAT data themselves by mapping the observed flow, together with the corotation motion of the radar, along undistorted model magnetic field lines to the equator. The flow component values used for this purpose are the most "typical" flow values for this data set in a particular MLT sector, obtained from the multivariate fit discussed. That is, the radar values are obtained from the minimum f fits to Eq. (1) for each flow component, with $\mathscr{V}^2B_S$ being taken to be the averaged value in the data set for that MLT sector, and IMF B_y being set to zero (since we are looking for the flow perturbations about the $B_y = 0$ state). These flow components (not inclusive of corotation) are shown together with the averaged values of $\mathscr{V}^2B_S$ employed versus MLT in Fig. 6a. The typical value of $\mathscr{V}^2B_S$ for the data set is ~ -2 nT. The flow components are also shown (again without the corotation component) in polar dial format in Fig. 6b. The flows are of the expected twin-vortex form, though the axis of approximate symmetry is rotated by ~ 2 h of MLT away from the noon-midnight meridian towards earlier local times, as noted in the previous section. This rotation is consistent with the results of previous statistical studies at EISCAT latitudes (e.g. Rich and Hairston, 1994; Weimer, 1995; Ruohoniemi and Greenwald, 1996).

We now map these flows, with added corotation, along undistorted field lines into the equatorial plane, assuming that the field lines are electric equipotentials. To do this we have employed the Tsyganenko (1989) field model (henceforth the "T89" model), simplified to the case of zero dipole tilt. The model is parametrised in terms of the Kp magnetic disturbance index, undifferentiated by + or − qualifiers. In Fig. 7 we show mappings of the EISCAT field lines, drawn from a magnetic latitude of 66.3° at 1 h intervals of MLT, for (from top to bottom) the $Kp = 0$, 1, 2, and 3 models. It can be seen that the field lines on the dayside change relatively little with Kp, being essentially those of an undisturbed dipole. On the nightside, however, the quasi-dipolar field lines present in the $Kp = 0$ model become increasingly tail-like as Kp increases, with major tail-like changes being present for $Kp = 3$. Examination of the Kp values for the intervals used in this study shows that the average modal value (undifferentiated by + or − qualifiers) of Kp is $Kp = 3$. Here, however, we will employ all four field models in order to examine the degree to which the results depend on the nature of the unperturbed field.

The mapping of the ionospheric flow into the equatorial plane along the model field lines is performed as follows. Suppose the averaged flow measured in a certain MLT interval has components v_E and v_N transverse to the ionospheric magnetic field. We assume that this flow is appropriate to the centre of the MLT interval concerned (in the rotating frame), at the magnetic latitude of EISCAT. To take account of the corotating motion of the radar around the dipole axis we also add a constant eastward corotation velocity of $v_C = 194.3$ m s^{-1} to these measurements, as appropriate to the magnetic latitude and height of the observation

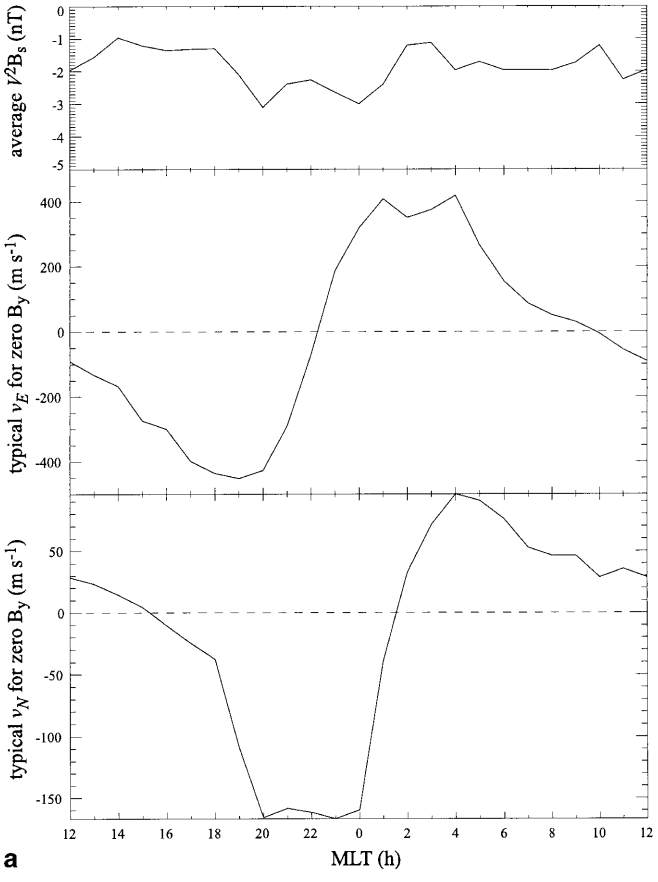

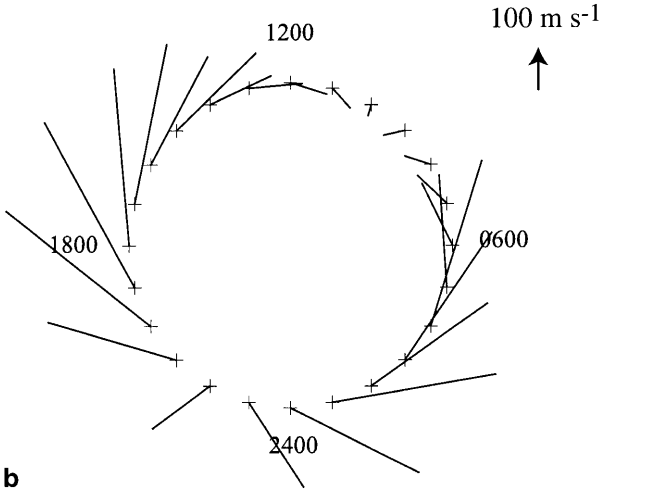

Fig. 6. a Shows the unperturbed "typical" ionospheric flows employed in our theoretical analysis versus MLT, obtained from the multivariate fits whose coefficients are shown in Fig. 4. The v_E and v_N component values shown in the *second* and *third panels*, respectively, have been computed using the averaged values of $\mathscr{V}^2B_S$ shown in the *upper panel*, and IMF B_y has been taken to be zero. Corotation, not included here, adds 194.3 m s^{-1} to the eastward component of the flow in the inertial frame. **b** Shows the "typical" flow components plotted in **a**, presented as vectors in a polar dial format, with noon at the *top* and dusk to the *left*. Corotation is again not included

point. We then set up a local coordinate system in the ionosphere whose origin is located at this observation "point", whose z axis is directed downwards along the magnetic field, with x pointing north and y east, both

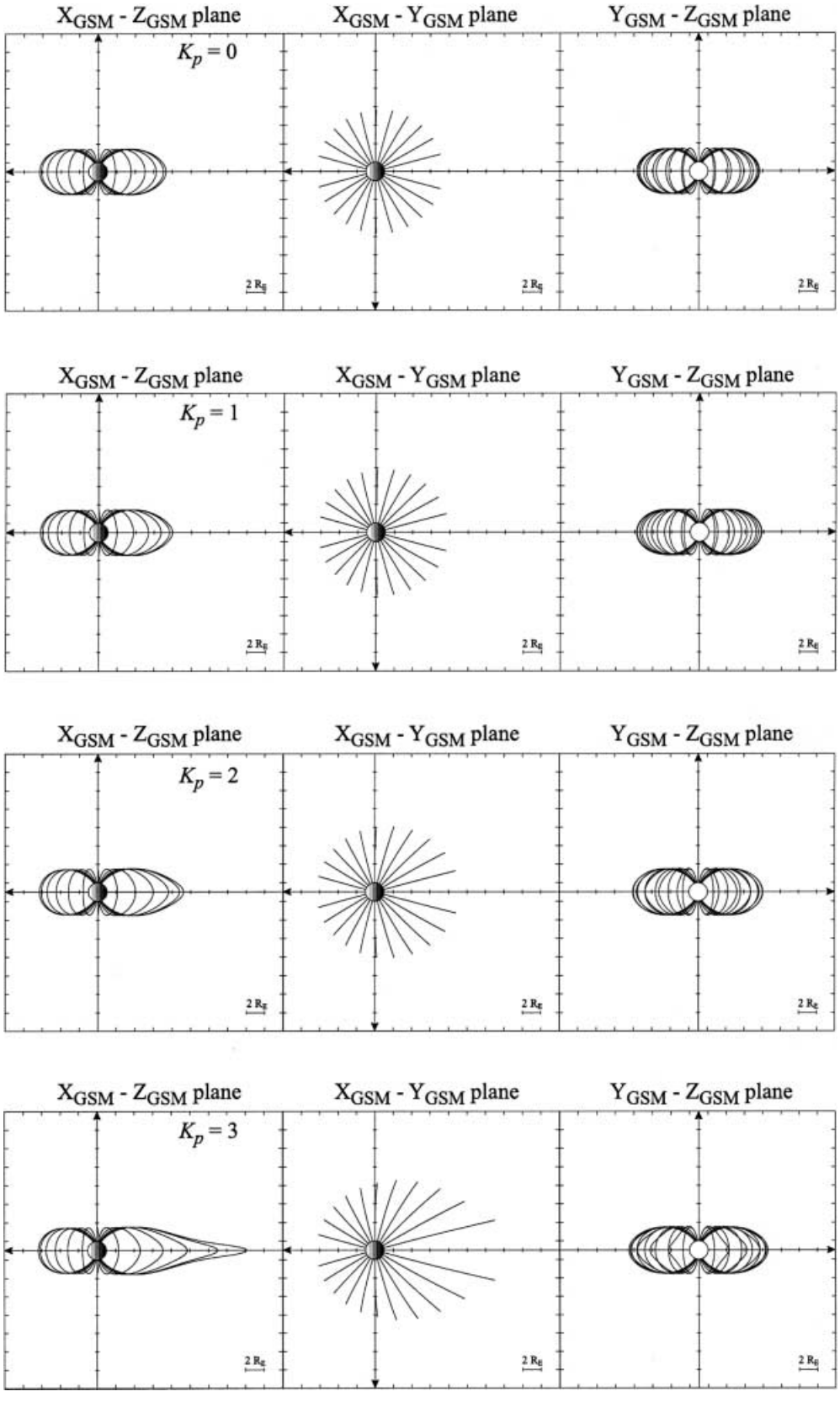

Fig. 7a–d. Plot of EISCAT field lines in GSM coordinates projected onto the *X–Z* (*left*), *X–Y* (*centre*), and *Y–Z* (*right*) planes, for (from *top* to *bottom*) the T89 **a** $Kp = 0$, **b** $Kp = 1$, **c** $Kp = 2$, and **d** $Kp = 3$ models, for zero dipole tilt. *Field lines* are drawn from 66.3° magnetic latitude at 1 h intervals of MLT

transverse to the field. The ionospheric electric field associated with the flow in the non-rotating frame is then

$$E_i = -v_i \times B_i = -v_E^* B_i \hat{x} + v_N B_i \hat{y} \ , \qquad (3)$$

where $v_E^* = v_E + v_C$, and B_i is the strength of the ionospheric magnetic field. If the ionospheric potential is then taken to be ϕ_{io} at the observation point (an arbitrary value), the potential elsewhere (locally) is

$$\phi_i(x,y) = \phi_{io} + (v_E^* x - v_N y)B_i \ . \tag{4}$$

We now take three points in the ionosphere and map them along the undistorted model field lines into the equatorial plane. These are "point 0" given by $(x_0,y_0)=(0,0)$, the observation point in the ionosphere, "point 1" displaced through distance Δ to the north such that $(x_1,y_1)=(\Delta,0)$, and "point 2" displaced through distance Δ to the east such that $(x_2,y_2)=(0,\Delta)$. The potentials at these points are then ϕ_{io}, $\phi_{io}+v_E^* B_i\Delta$, and $\phi_{io}-v_N B_i\Delta$, respectively. We now set up another local coordinate system in the equatorial plane whose origin is at the mapped observation point, corresponding to "point 0" in the ionosphere, whose X axis points towards the Sun and whose Y axis points to dusk, both transverse to the northward equatorial field. Let us then suppose that "point 1" in the ionosphere maps to (X_1,Y_1) in the equatorial plane, and "point 2" to (X_2,Y_2), determined by numerical integration of the model field lines. From the assumed equipotentiality of the field lines we know that the potentials at the mapped points in the equatorial plane are the same as the potentials at the corresponding points in the ionosphere. If we then assume that the equatorial potential is given locally by

$$\phi_m(X,Y) = \phi_{io} + \left.\frac{\partial\phi_m}{\partial X}\right|_0 X + \left.\frac{\partial\phi_m}{\partial Y}\right|_0 Y \ , \tag{5}$$

equivalent to assuming a locally uniform equatorial electric field, we can then determine the differential coefficients by knowing the values of the potentials at mapped equatorial points 1 and 2. Simple manipulation yields

$$\left.\frac{\partial\phi_m}{\partial X}\right|_0 = \frac{(Y_1 v_N + Y_2 v_E^*)B_i\Delta}{(X_1Y_2 - X_2Y_1)} \ , \tag{6a}$$

and

$$\left.\frac{\partial\phi_m}{\partial Y}\right|_0 = -\frac{(X_1 v_N + X_2 v_E^*)B_i\Delta}{(X_1Y_2 - X_2Y_1)} \ . \tag{6b}$$

Equations (5) and (6) thus define the equatorial electrostatic potential local to the mapped observation point in the non-rotating frame. The equatorial plasma velocity at the mapped observation point is then given by

$$v_m = (v_{m_X}, v_{m_Y}) = \frac{1}{B_m}\left(-\left.\frac{\partial\phi_m}{\partial Y}\right|_0, \left.\frac{\partial\phi_m}{\partial X}\right|_0\right) \ , \tag{7}$$

where B_m is the equatorial field strength at the mapped observation point. These velocities are presented as vectors in the equatorial plane for all four T89 Kp models in Fig. 8, where results for the mapped "typical" flows plus corotation are shown. To obtain these results we have employed a value of Δ in the calculations which is sufficiently small that the results become, for practical purposes, independent of its value. Empirical investigation indicates that this condition is satisfied at EISCAT latitudes for Δ = 10 km (corresponding to $\sim 0.1^\circ$ of latitude), and this value has been employed throughout. In each case the flow vectors are plotted at the EISCAT observation point mapped to the equator along the model field, while the circle shows the dipole mapping (to 6.2 R_E), thus indicating the degree of field distortion away from the dipole in the model. The equatorial velocities so derived show a principally sunward flow, as expected. The vectors are also typically tilted towards dawn, except in the noon sector, where the corotation effect produces a tilt towards dusk. The more significant variation, however, concerns the nightside flows, which increase with Kp and become more sunward-directed as the nightside field becomes more tail-like and displaced away from the dipole mapping. For example, the equatorial flow on EISCAT field lines near midnight increases by a factor of $\sim$2 from the $Kp=0$ to the $Kp=2$ model, and by a further factor of $\sim$8 from $Kp=2$ to $Kp=3$ (note the change of velocity scale in the latter plot). This effect is due to the reducing value of the equatorial field strength B_m at the mapped point as the model field becomes more tail-like (see Eq. 7).

Having thus derived the local equatorial potential (or equivalently the equatorial flow), we can now map it back into the ionosphere along model magnetic field lines which are distorted by the presence of an IMF B_y-dependent perturbation field, thus determining the corresponding perturbation flow in the ionosphere. Following the earlier studies by Cowley and Hughes (1983) and Nagai (1987), Wing *et al.* (1995) have used $\sim$5 years of data from the GOES-6 and -7 spacecraft to show that the B_y perturbation field at geostationary orbit varies from $\sim$0.3 of IMF B_y at noon, to $\sim$0.8 of IMF B_y at midnight. Here we have adopted their values, and have assumed that for a +1 nT B_y field in the interplanetary medium, a B_y perturbation field exists on nominally near-geostationary EISCAT field lines which varies sinusoidally with MLT from a minimum value of 0.3 nT at noon to a maximum value of 0.8 nT at midnight. That is, the perturbation field for 1 nT of IMF B_y is given by

$$B_y = (0.55 - 0.25\cos\psi)\,\text{nT} \ , \tag{8}$$

where ψ is the azimuthal angle measured from noon.

Using this perturbation field in the magnetosphere, the perturbed flows in the ionosphere are calculated in the following way. We map along the distorted magnetic field lines from points 0, 1, and 2 in the ionosphere, defined as before, to the equatorial plane. Suppose the equatorial coordinates of these field lines in the local $(X,\ Y)$ system are now found to be (X_0,Y_0), $(X_0+X_1',\ Y_0+Y_1')$, and (X_0+X_2', Y_0+Y_2'), respectively. Then assuming the equatorial potential function is fixed locally via Eqs. (5) and (6), we find the potentials at points 1 and 2, ϕ_{m1}' and ϕ_{m2}', relative to the potential at point 0, ϕ_{m0}' to be given by

$$\phi_{m1}' = \phi_{m0}' + \left.\frac{\partial\phi_m}{\partial X}\right|_0 X_1' + \left.\frac{\partial\phi_m}{\partial Y}\right|_0 Y_1' \tag{9a}$$

and

$$\phi_{m2}' = \phi_{m0}' + \left.\frac{\partial\phi_m}{\partial X}\right|_0 X_2' + \left.\frac{\partial\phi_m}{\partial Y}\right|_0 Y_2' \ . \tag{9b}$$

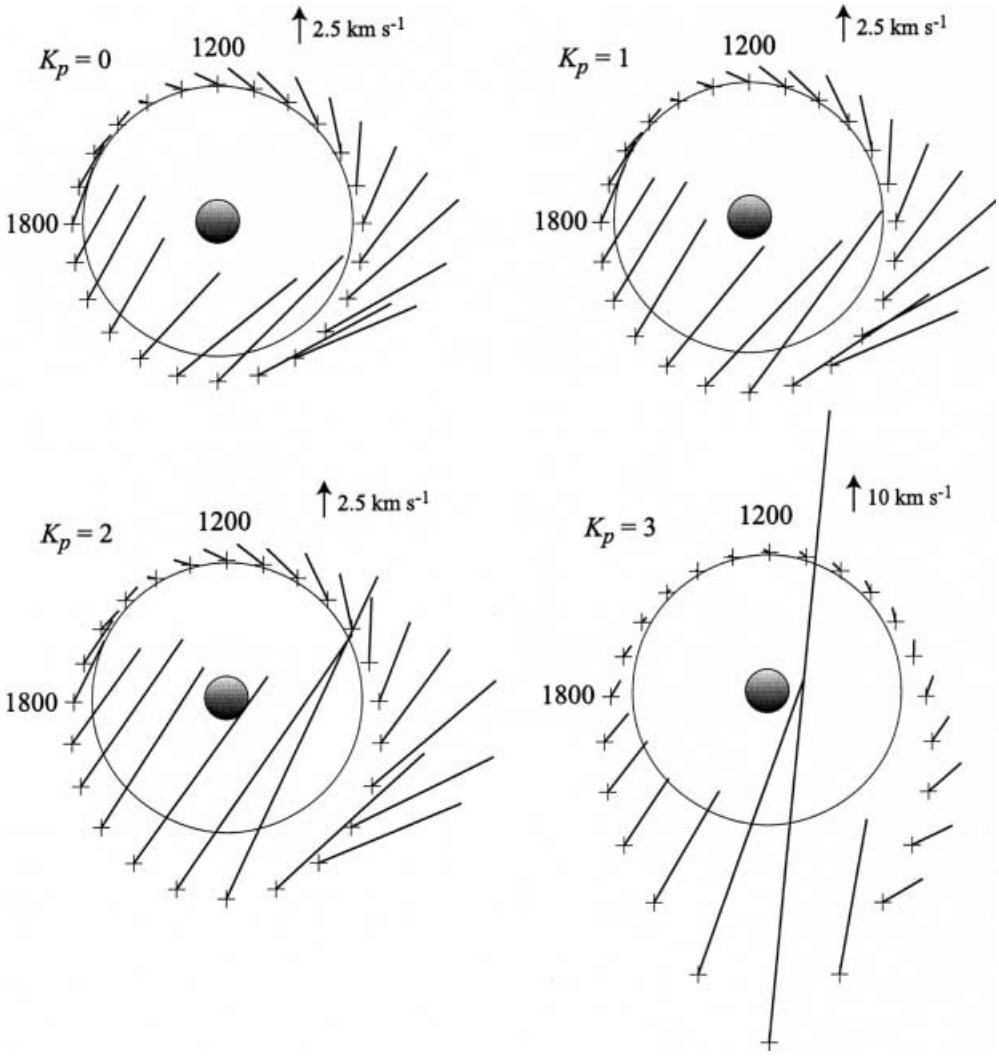

Fig. 8. Flow vectors in the magnetospheric equatorial plane derived by mapping the EISCAT "typical" velocities for zero IMF B_y, plus an added eastward corotation flow about the dipole axis, along equipotential model magnetic field lines to the equator. Results are shown using the EISCAT flows mapped using the T89 $Kp = 0$, 1, 2, and 3 models as indicated. In each plot noon is at the *top* and dusk to the *left*

Since the distorted field lines are also assumed to be equipotentials, these are also the potentials in the ionosphere at points 1 and 2, relative to point zero. Consequently, the perturbed velocity components in the ionosphere are given by

$$v'_N = -\frac{(\phi'_{m2} - \phi'_{m0})}{B_i \Delta} = -\frac{1}{B_i \Delta}\left(\frac{\partial \phi_m}{\partial X}\bigg|_0 X'_2 + \frac{\partial \phi_m}{\partial Y}\bigg|_0 Y'_2\right) \tag{10a}$$

and

$$v^{*\prime}_E = \frac{(\phi'_{m1} - \phi'_{m0})}{B_i \Delta} = \frac{1}{B_i \Delta}\left(\frac{\partial \phi_m}{\partial X}\bigg|_0 X'_1 + \frac{\partial \phi_m}{\partial Y}\bigg|_0 Y'_1\right) . \tag{10b}$$

Substituting for the derivatives from Eq. (6) finally yields the following expressions for the perturbed velocity components

$$v'_N = \frac{v_N(X_1 Y'_2 - X'_2 Y_1) + v^*_E(X_2 Y'_2 - X'_2 Y_2)}{(X_1 Y_2 - X_2 Y_1)} \tag{11a}$$

and

$$v^{*\prime}_E = \frac{v^*_E(X'_1 Y_2 - X_2 Y'_1) + v_N(X'_1 Y_1 - X_1 Y'_1)}{(X_1 Y_2 - X_2 Y_1)} . \tag{11b}$$

The perturbed ionospheric flows v'_N and $v^{*\prime}_E$ are thus determined in terms of the measured flows and the displacements of the mapped field lines in the equatorial plane. The velocity perturbations are then given by the following differences

$$\delta v_N = v'_N - v_N = \frac{v_N(X_1(Y'_2 - Y_2) - (X'_2 - X_2)Y_1) + v_E(X_2 Y'_2 - X'_2 Y_2)}{(X_1 Y_2 - X_2 Y_1)} \tag{12a}$$

and

$$\delta v_E = v^{*\prime}_E - v^*_E = \frac{v^*_E((X'_1 - X_1)Y_2 - X_2(Y'_1 - Y_1)) + v_N(X'_1 Y_1 - X_1 Y'_1)}{(X_1 Y_2 - X_2 Y_1)} . \tag{12b}$$

We note that these velocity perturbations are linearly proportional to the perturbation B_y field applied,

provided the latter remains small compared with the unperturbed field along the model EISCAT field lines. The validity of linearity for the conditions of interest here has been examined by direct evaluation of these formulae on nightside field lines (for which breakdown is most likely) using perturbation B_y fields over a range of several nT. The results for the $Kp = 0$–2 models were found to be very closely linear over this range, and for the $Kp = 3$ model approximately so (because the applied perturbation fields then become comparable with the weak equatorial nightside fields of the undisturbed model). If we then evaluate δv_E and δv_N using a distorted magnetic field which corresponds to +1 nT B_y in the interplanetary medium, i.e. using the magnetospheric perturbation field given by Eq. (8), then the values derived represent the change in the flow components per nT of IMF B_y. These values thus represent the theoretical counterpart of the IMF B_y-related gradient vectors obtained from the coefficients g_y in the previous section, and shown in Figs. 4 and 5, which show the observed change in the flow components per nT of IMF B_y.

5 Theoretical results

Before describing the results obtained by mapping the "typical" flows at EISCAT for zero IMF B_y (plus corotation) along distorted field lines, it is instructive first to consider the effects associated with each unperturbed flow component separately. We note from Eq. (12) that for a particular field mapping, the difference flows δv_E and δv_N are given by a linear combination of terms proportional to v_E and v_N. In Fig. 9 we thus take an unperturbed flow with a northward component of $v_N = 100$ m s^{-1} at all MLT, and zero v_E. We note that this sense of v_N is appropriate to the geophysical case on the dayside, but is generally opposite on the nightside. For simplicity we also take a constant +1 nT perturbation B_y field at all MLT. In Fig. 9a we plot the difference velocity components δv_E (upper panel) and δv_N (lower panel) determined from Eq. (12), versus MLT (like Fig. 4, centred on midnight). The dash-double-dot lines show results for the $Kp = 0$ model, the dash-dot lines $Kp = 1$, the short-dashed lines $Kp = 2$, and the long-dashed lines $Kp = 3$. Considering first the results for δv_E in the upper panel, the east–west difference flows are directed eastward by day and westward by night, and are near zero on the dawn-dusk meridian, in conformity with the discussion given in the introduction. If we consider the noon-midnight meridian, for example, an unperturbed northward flow in the ionosphere corresponds to an exactly radial flow away from the Earth in the equatorial plane at both noon and midnight. As we move along these magnetospheric streamlines in the distorted field case, the ionospheric footprint in the Northern Hemisphere (which is also a streamline) moves poleward and increasingly to the east at noon, and poleward and increasingly to the west at midnight, as in Fig. 1, hence giving rise to the east–west difference flows shown in the figure. In the geophysical case, of course, the generally poleward flows by day and equatorward flows at night both give rise to an eastward difference flow, as we previously discussed. It can be seen in Fig. 9a, however, that for a constant unperturbed northward flow, and a fixed perturbation B_y field (1 nT), the east–west difference flows are much larger by night than by day for all the field models considered here. The nightside difference flows also increase strongly with increasing Kp, particularly for the $Kp = 3$ model. Values peak at midnight at -7 m s^{-1} for the $Kp = 0$ model, -13 m s^{-1} for $Kp = 1$, -29 m s^{-1} for $Kp = 2$, and -406 m s^{-1} for $Kp = 3$, compared with a value of $\sim$1 m s^{-1} at noon for all models. This day-night asymmetry, and the increasing nightside effects with increasing Kp, are due to the increasingly tail-like fields in the model on the nightside with increasing Kp. As the model field lines become more distended with Kp, and the equatorial fields weaker and more comparable in magnitude with the perturbation B_y field, so the field distortion effects and the velocity perturbations become increasingly large.

The north–south difference flow, δv_N, is shown versus MLT in the lower panel of Fig. 9a. Values are positive on the dusk side and negative on the dawn side, and again much larger by night than by day. More significantly, however, noting the change in scales between the upper and lower panels of the figure, they are in all cases much smaller than the differences in the east–west flow component, and are generally negligibly small. Overall, therefore, the dominant effect is in the zonal component of the flow, and the latitudinal component is generally negligible. This conclusion is illustrated directly in Fig. 9b where we show the perturbation velocities as vectors in polar dial format for all four Kp models. These vectors point almost directly westward by night and eastward by day (for northward unperturbed flow and a positive added B_y field), the dayside vectors being only just visible on the low-Kp model plots, illustrating the strong day-night asymmetry in the effect. The nightside vectors become increasingly large with Kp (note the changes in scale from plot to plot), with the largest values being concentrated near midnight where the model field is most tail-like at EISCAT latitudes.

In Fig. 10 results are shown in the same format for an assumed eastward flow $v_E = 100$ m s^{-1} at all MLT, and zero v_N. We note that this flow has the same sense as the corotation flow (but is a factor of $\sim$2 less in magnitude), while with respect to the solar wind-driven flows it has the same sense as the geophysical case at dawn, but is opposite at dusk. The perturbation field is again a constant +1 nT B_y field at all MLT. In this case, the east–west difference component, δv_E, shown in the upper panel of Fig. 10a, is directed westward at dusk (weakening the unperturbed flow), and eastward at dawn (strengthening the unperturbed flow). As previously discussed in the introduction, this effect is due to the dawnward shift of the feet of the field lines near the dawn-dusk meridian in the Northern Hemisphere for B_y positive, as seen in Fig. 1. Because this shift increases with latitude, it "expands" the auroral zone flow over a greater latitude range at dusk, and hence weakens it,

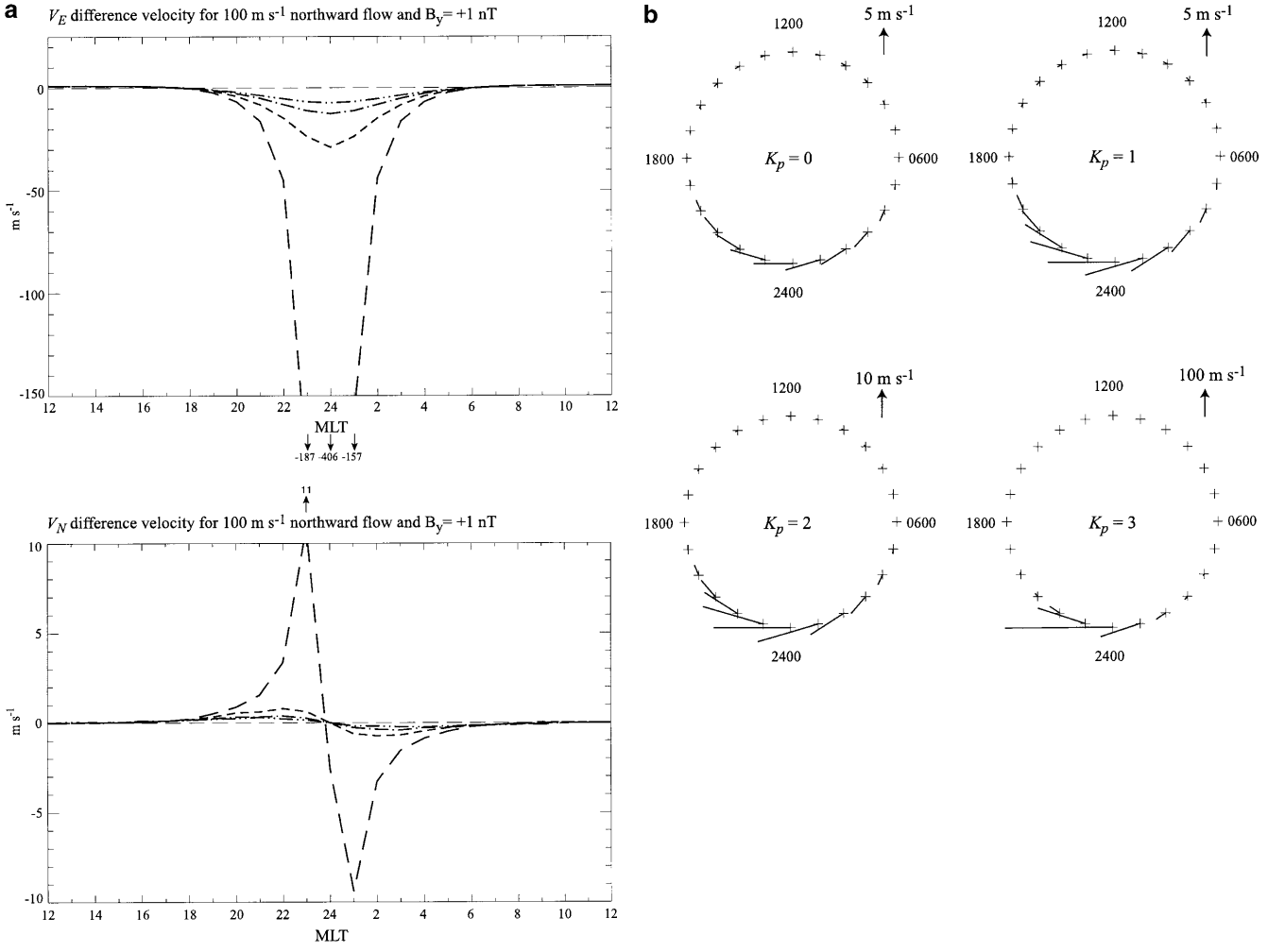

Fig. 9a, b. Theoretical difference flow components in the Northern Hemisphere obtained from Eqs. (12), for the case in which the unperturbed flow has been taken to be a poleward flow of 100 m s^{-1} at all local times, with zero eastward flow. The magnetospheric perturbation field has been taken to be a positive B_y field of 1 nT. In **a**, the two perturbation flow components are plotted versus MLT (centred on midnight), with δv_E being shown in the *upper panel* and δv_N in the *lower*. Note the *change of scale* between the panels. The *dash-double-dot lines* show results for the T89 $Kp = 0$ model, the *dash-dot lines* $Kp = 1$, the *short-dashed lines* $Kp = 2$, and the *long-dashed lines* $Kp = 3$. In **b**, the difference flow vectors are shown in a polar dial format with noon at the *top* and dusk to the *left*. Note the change in velocity scale from plot to plot

while "compressing" the flow over a narrower latitude range at dawn, and hence strengthening it. The opposite effects in the Southern Hemisphere produce an inter-hemispheric differential zonal flow which tilts the field lines out of the magnetic meridian as they propagate azimuthally around the Earth, the tilt being just that required by the presence of the perturbation B_y field. As before, the perturbation flows are stronger by night than by day, due to the day-night asymmetry in the T89 model, and peak ~3 h of MLT before and after midnight rather than near the dawn-dusk meridian. The north–south difference component, δv_N, shown in the lower panel of Fig. 10a is an order of magnitude smaller than δv_E, and near the noise level of the calculation (difference flows of ~0.1 m s^{-1}). Hence, as is also clear from the polar dial vector plots shown in Fig. 10b, the difference velocities associated with an unperturbed east–west flow are also predominantly zonal, like those associated with an unperturbed v_N flow shown previously in Fig 9. However, the magnitude of the effect is less than a tenth of that associated with v_N, for the same magnitude of unperturbed flow and the same perturbation B_y field. Values peak in the pre- and post-midnight sectors at ~1 m s^{-1} for the $Kp = 0$ and $Kp = 1$ models, ~2 m s^{-1} for $Kp = 2$, and ~4 m s^{-1} for $Kp = 3$. However, because in the geophysical case the solar wind-driven east–west flows near dawn and dusk are larger than the north–south flows near noon and midnight by factors of ~5 (see Fig. 4), this effect will still contribute at modest levels.

Overall, therefore, these preparatory results show that the principal difference velocities are those associated with the unperturbed north–south flow. They are predominantly zonal, and for the usual geophysical situation of poleward flows by day and equatorward flows by night are directed eastward in both cases for a positive B_y perturbation field, with maxima at noon and midnight, and zeros near dawn and dusk. However,

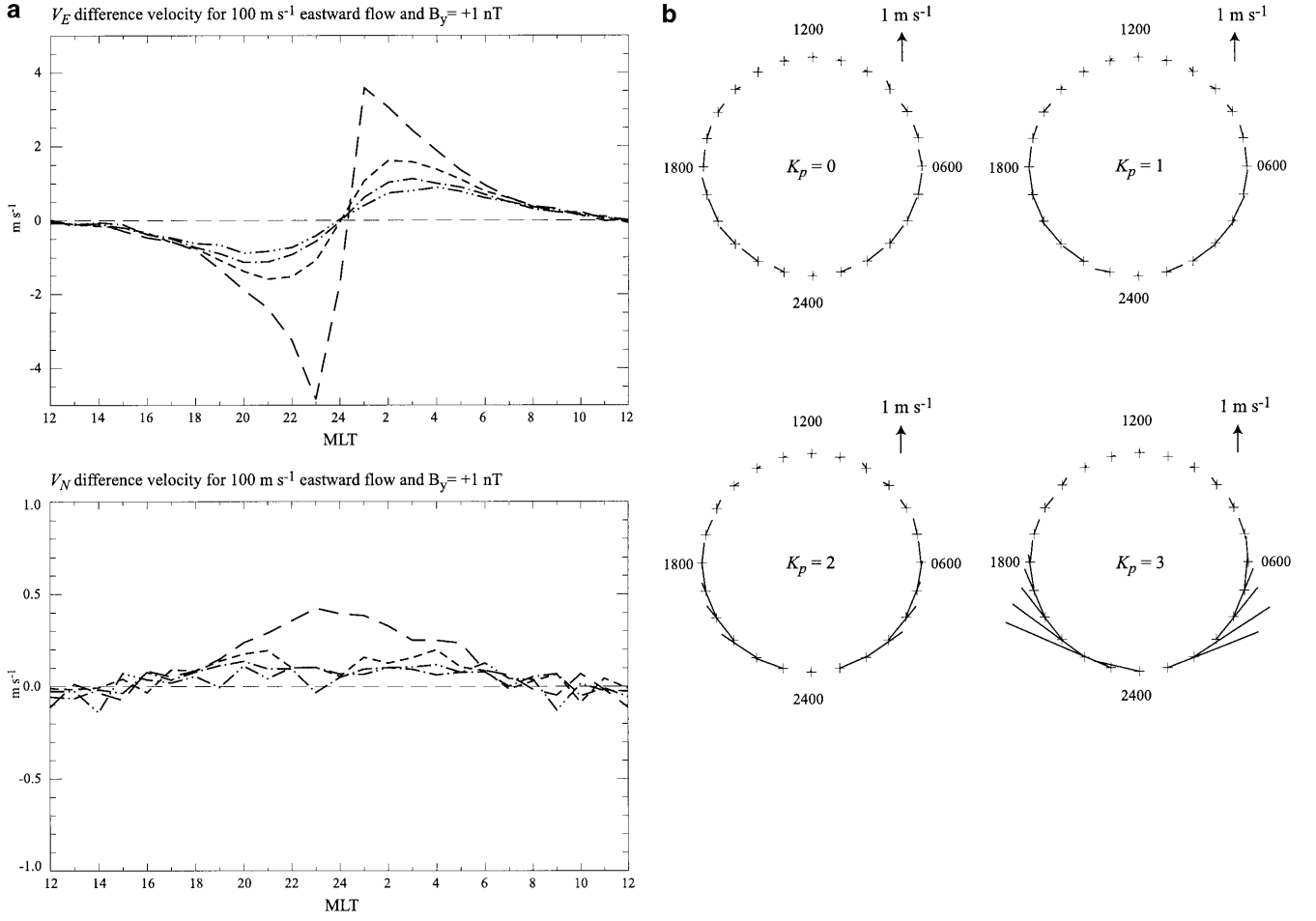

Fig. 10a, b. As for Fig. 9 except that the unperturbed flow has been taken to be an eastward flow of 100 m s^{-1} at all local times, with zero northward flow. The magnetospheric perturbation field has again been taken to be a positive B_y field of 1 nT. Note also the difference in the velocity scales compared with Fig. 9

because of the noon-midnight asymmetry in the background field, the effects on the dayside are much smaller than those on the nightside, and are generally of negligible amplitude. The difference velocities associated with the unperturbed east–west flow are also predominantly zonal. Given the usual geophysical situation of a westward unperturbed flow at dusk and an eastward unperturbed flow at dawn, the difference velocities are again directed eastward for a positive B_y perturbation field, though corotation will introduce an asymmetry by adding to the effect at dawn while subtracting from it at dusk. This difference flow is intrinsically weaker than that associated with the unperturbed north–south flow. However, because it is essentially in quadrature with the MLT phasing of the north–south flow effect, with zeros near noon and midnight and peaks between, it may be of some significance near dawn and dusk where the velocity perturbations associated with the unperturbed north–south flow are small.

With this introduction, we now finally turn to the main results, the difference flow vectors derived using the "typical" EISCAT flows for zero IMF B_y shown in Fig. 6, together with the sinusoidally varying magnetospheric perturbation B_y field given by Eq. (8), which we take to correspond to a +1 nT. B_y field in the interplanetary medium. As previously pointed out, these difference velocities then represent our theoretical estimates of the B_y-related velocity gradient vectors obtained from the g_y coefficients of our fits to the EISCAT data, as shown in Figs. 4 and 5. Theoretical results based on "typical" EISCAT flows for zero IMF B_y conditions (plus corotation) are shown in Fig. 11, in the same format as Figs. 9 and 10. All four T89 field models are again employed in order to demonstrate the dependence of the results on the unperturbed magnetic field structure. The eastward difference component, shown in the upper panel of Fig. 11a, is positive at all MLT, but again much stronger by night than by day. Peak values at midnight depend strongly on the model field, reaching a value of 12 m s^{-1} (per nT of IMF B_y) for the $Kp = 0$ model, 20 m s^{-1} for $Kp = 1$, 46 m s^{-1} for $Kp = 2$, and 642 m s^{-1} for $Kp = 3$. By comparison, values at noon are less than 1 m s^{-1}, of negligible amplitude. The nightside flows are also seen to be somewhat asymmetrical in form about midnight, with generally larger values pre-midnight than post-midnight. Since the main contribution to the zonal

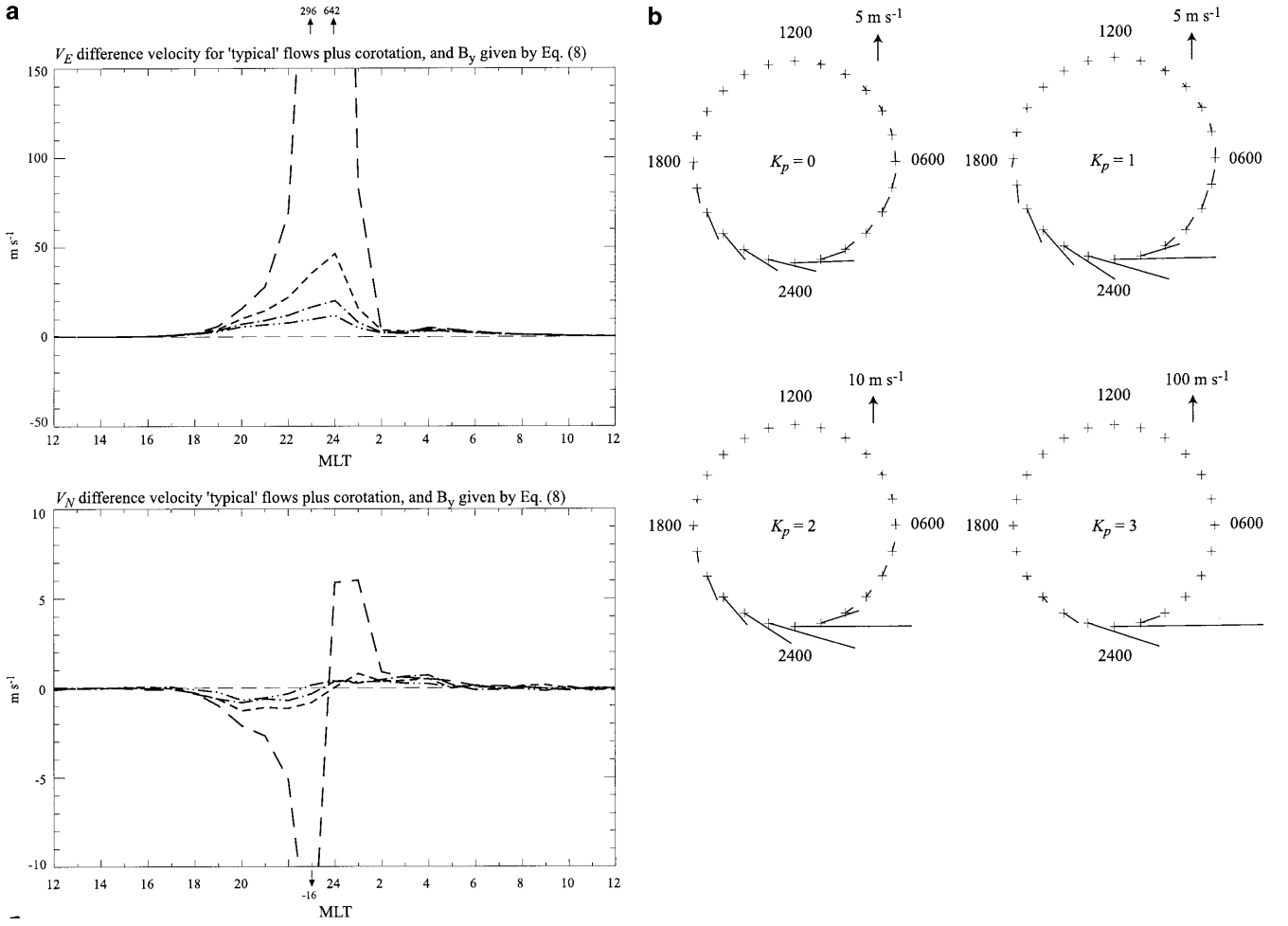

Fig. 11a, b. Difference flow vectors in the Northern Hemisphere corresponding to a +1 nT B_y field in the interplanetary medium (the internal perturbation field being given by Eq. 8), where the unperturbed flow has been taken to be the "typical" EISCAT flow (corresponding to zero IMF B_y). The format is the same as in Fig. 9

difference flow comes from the effect associated with the north–south component of the unperturbed flow, this asymmetry has its origin in the MLT-dependence of the unperturbed v_N component at EISCAT. Examination of the "typical" flows displayed in Fig. 6a shows that the equatorward flow on the nightside peaks not at midnight, but in the pre-midnight Harang sector, and then reverses to a poleward flow in the post-midnight sector, beyond ~0200 MLT. The zonal difference velocity associated with this component therefore tends to be enhanced pre-midnight, and reverses to become relatively small but westward between 0200 and 0600 MLT. The zonal flow associated with the unperturbed east–west component (which includes the corotation flow) then adds a weak eastward flow in the dusk sector which reverses to a weak westward flow pre-midnight, and a stronger eastward flow post-midnight (see the upper panel of Fig. 10a). This modestly extends the MLT region over which the eastward flows are significant towards both dusk and dawn, in particular cancelling and reversing the post-midnight westward flows that result from the unperturbed north–south flow effect alone.

These results can be compared quantitatively with the observed IMF B_y-related gradients for v_E shown in Fig. 4a. It can be seen that a reasonable measure of agreement has been achieved, concerning the sense of the effect and the large day-night asymmetry. The theory indicates that significant perturbation flows should be confined between ~2000 and ~0200 MLT, in good agreement with the main region of non-zero g_y values shown in Fig. 4a, between ~2100 and ~0300 MLT. The theory does not account, however, for the smaller additional effect observed in the data in the pre-dusk hours. With regard to the absolute magnitude of the effect, it can be seen that good agreement is obtained for the modestly distorted tail-like fields of the $Kp = 1$ and 2 models, which give peak values of ~20–40 m s^{-1} (per nT of IMF B_y), similar to those observed. The $Kp = 3$ model clearly produces values which are far too large, by an order of magnitude, indicating that the nightside field distortion in the magnetic model is far from typical of EISCAT field lines.

Results for the north–south component of the difference flow are shown in the lower panel of Fig. 11a. These are again dominated by the effect associated with the north–south component of the unperturbed flow shown in Fig. 9, and for the generally equatorward flow at night gives equatorward difference flows pre-midnight

and poleward flows post-midnight. However, these are much smaller than the zonal difference flows discussed already, with peak amplitudes for the $Kp = 0$–2 models of $\sim$1 m s^{-1} (per nT of IMF B_y). Such amplitudes are very small compared with those in v_E, and agree with the observed gradients in Fig. 4b in the sense that both indicate the presence of negligible IMF B_y-related effects in the north–south component of the flow.

Finally, in Fig. 11b these theoretical perturbation flows for a +1 nT IMF B_y field are shown as vectors in a polar dial format, so that they may be compared with the corresponding presentation of EISCAT results shown in Fig. 5. The overall agreement seems reasonable. The theoretical results correctly give the direction of the main component of the perturbation flow, principally eastward for positive IMF B_y, the strong day-night asymmetry, and, for the less distorted models, a reasonable estimate of the magnitude of the effect, of a few tens of m s^{-1} nT^{-1}. As indicated, the principal discrepancy lies the lack of explanation of the smaller effect observed at dusk.

6 Summary

We have employed a database of $\sim$300 h of tristatic ionospheric velocity data obtained overhead at Tromsø (66.3° magnetic latitude) by the EISCAT UHF radar system, and have analysed them for the presence of flow effects associated with the y-component of the IMF. In common with the findings of previous statistical studies of data from both polar orbiting spacecraft and ground-based radar, we find that such effects are indeed present. Since it has already been established by Khan and Cowley (1999) that the EISCAT flows respond to IMF B_z, we have undertaken a linear least-squares multivariate analysis in which the flow responses to IMF B_y and B_z (specifically the "half wave rectifier" function $\mathscr{V}^2 B_S$) have been determined simultaneously. With regard to the variation with respect to IMF B_z, the results confirm, and are in accord with, the results of Khan and Cowley (1999). In addition, the results derived here also show the presence of perturbation flows associated with IMF B_y. For positive IMF B_y the perturbation flows are directed principally eastward, with negligible north–south components, and occur in two adjacent local time sectors. The principal sector lies on the nightside between $\sim$2100 and $\sim$0300 MLT, thus being centred on midnight. The magnitude of the east–west perturbation flow in this sector is 20–40 m s^{-1} nT^{-1}. The variation in the east–west flow over the usual range of IMF B_y ($\sim \pm 5$ nT) due to this effect is thus $\sim$200–400 m s^{-1}, which is therefore significant compared with averaged flows of $\sim$300–500 m s^{-1}. A similar but smaller (10–20 m s^{-1} nT^{-1}) effect is observed in the pre-dusk sector, at $\sim$1600–1700 MLT. At other local times no IMF B_y-dependence is observed within the uncertainty estimates (i.e. values are $\sim$5 m s^{-1} nT^{-1} or less), this situation applying in the pre-dawn sector and over most of the dayside.

The presence of oppositely-directed IMF B_y-related perturbation flows in the Northern and Southern Hemispheres (as indicated by previous studies), raises issues of magnetic conjugacy in the closed field line EISCAT regime investigated here. We have thus considered whether the observed perturbation flows can be accounted for quantitatively by a model in which the equatorial flow in the inner magnetosphere is independent of IMF B_y, but where the flow perturbations are produced by distortions of the magnetospheric magnetic field associated with a "penetrating" component of the IMF B_y field. We have thus set up a theoretical model in which the EISCAT flows for zero IMF B_y, plus corotation, are mapped to the equator along undistorted magnetic field lines (given by the T89 model) to provide an estimate of the equatorial flow, and are then mapped back to the ionosphere along distorted field lines to determine the magnitude and direction of the flow perturbations thereby produced. The field distortion employed is simply due to an added B_y field whose amplitude is a fraction of the IMF B_y, varying with MLT, which is based on measurements at geostationary orbit (nearby nominal EISCAT field lines). The principal effect produced is the appearance of east–west perturbation flows in the noon and midnight sectors whose sense is determined by the north–south component of the unperturbed flow, and which in the geophysical case are generally directed eastward in the Northern Hemisphere for IMF B_y positive. However, the model perturbation flows are much larger on the nightside than on the dayside, as observed, due principally to the day-night asymmetry of the magnetospheric field. East–west perturbation flows are also present in the dawn and dusk sectors whose sense is determined by the east–west component of the unperturbed flow (including corotation), and which in the geophysical case are again generally directed eastward in the Northern Hemisphere for IMF B_y positive. However, these are generally smaller than the flow effects associated with the unperturbed north–south flow, and contribute only at modest levels at EISCAT latitudes.

Theoretical results have been derived starting from "typical" ionospheric flows at EISCAT for zero IMF B_y (obtained from the multivariate fits), to which corotation has been added, which can be directly compared with the observed flow perturbations. The model results are found to account well for the observed effects in the midnight sector, in terms of the direction and sense of the flow, and their local time extent. The magnitude of the effect also agrees with the observations for the low-Kp magnetic models. The high Kp magnetic model ($Kp = 3$) produces theoretical values which are too large by an order of magnitude, indicating that the nightside distension of the field in the model is far from typical at EISCAT latitudes. The model does not reproduce the lesser IMF B_y-related flow effects observed in the pre-dusk sector. Although the model indicates the presence of eastward-directed perturbation flows in this sector for positive IMF B_y, as observed, their amplitude is much smaller than those observed. The perturbation magnetic fields in the magnetosphere in this sector must be much

larger than those employed in the present model if these flow perturbations are to be explained in terms of the theory proposed here.

Acknowledgements. The authors would like to thank the Director of EISCAT and his staff for operating the facility and providing the EISCAT radar data. EISCAT is an international association supported by the research councils of Finland (SA), France (CNRS), Germany (MPG), Japan (NIPR), Norway (NAVF), Sweden (NFA), and the United Kingdom (PPARC). The IMP-8 magnetometer data (Principal Investigator: R.P. Lepping) were provided by the National Space Science Data Center, while the fine resolution plasma data (Principal Investigator: A.J. Lazarus) were provided by the Massachusetts Institute of Technology. This work was performed while one of us (HK) was supported by a studentship provided by the University of Leicester.

Topical Editor Denis Alcayde thanks G. Ghislam and another referee for their help in evaluating this paper.

References

Cowley, S. W. H., Magnetospheric asymmetries associated with the *Y*-component of the IMF, *Planet. Space Sci.*, **29,** 79, 1981.

Cowley, S. W. H., and W. J. Hughes, Observations of an IMF sector effect in the *Y* magnetic field component at geostationary orbit, *Planet. Space Sci.*, **31,** 73, 1983.

Cowley, S. W. H., J. P. Morelli, and M. Lockwood, Dependence of convective flows and particle precipitation in the high-latitude ionosphere on the *X* and *Y* components of the interplanetary magnetic field, *J. Geophys. Res.*, **96,** 5557, 1991.

Crooker, N. U., Dayside merging and cusp geometry, *J. Geophys. Res.*, **84,** 951, 1979.

Dungey, J. W., Interplanetary field and the auroral zone, *Phys. Res. Lett.*, **6,** 47–48, 1961.

Etemadi, A., S. W. H. Cowley, M. Lockwood, B. J. I. Brumage, D. M. Willis, and H. Lühr, The dependence of high-latitude dayside ionospheric flows on N–S component of IMF: a high-time resolution correlation analysis using EISCAT 'Polar' and AMPTE-UKS and IRM data, *Planet. Space Sci.*, **36,** 471, 1988.

Friis-Christensen, E., and J. Wilhjelm, Polar cap currents for different directions of the interplanetary magnetic field in the *y–z* plane, *J. Geophys. Res.*, **80,** 1248, 1975.

Galperin, Y. I., V. N. Ponomarev, and A. G. Zosimova, Equatorial ionospheric anomaly and interplanetary magnetic field, *J. Geophys. Res.*, **83,** 4265, 1978.

Heelis, R. A., Ionospheric convection at high latitudes, in *Magnetospheric boundary layers*, ESA SP-148, ESTEC, Noordwijk, The Netherlands, 75, 1978.

Heppner, J. P., Polar cap electric field distributions related to the interplanetary magnetic field direction, *J. Geophys. Res.*, **27,** 4877, 1972.

Heppner, J. P., and N. C. Maynard, Empirical high-latitude electric field models, *J. Geophys. Res.*, **92,** 4467, 1987.

Holzworth, R. H., and C.-I. Meng, Auroral boundary variations and the interplanetary magnetic field, *Planet. Space Sci.*, **32,** 25, 1984.

Iijima, T., R. Fujii, T. A. Poterma, and N. A. Saflekos, Field-aligned currents in the south polar cusp and their relationship to the interplanetary magnetic field, *J. Geophys. Res.*, **83,** 5595, 1978.

Jørgensen, T. S., E. Friis-Christensen, and J. Wilhjelm, Interplanetary magnetic field and high-latitude ionospheric currents, *J. Geophys. Res.*, **77,** 1976, 1972.

Khan, H., and Cowley, S. W. H., Observations of the response time of high latitude ionospheric convection to variations in the interplanetary magnetic field using EISCAT and IMP-8 data, *Ann. Geophysicae*, **17,** 1306, 1999.

Lockwood, M., The excitation of ionospheric convection, *J. Atmos. Terr. Phys.*, **53,** 177, 1991.

Lockwood, M., Solar wind-magnetosphere coupling, *Proc. EISCAT Internat. School in Corsica*, Ed. D. Alcaydé, 1995.

McDiarmid, I. B., J. R. Burrows, and M. D. Wilson, Magnetic field perturbations in the dayside cleft and their relationship to the IMF, *J. Geophys. Res.*, **83,** 5753, 1978.

Nagai, T., Interplanetary magnetic field B_y effects on the magnetic field at synchronous orbit, *J. Geophys. Res.*, **92,** 11 215, 1987.

Newell, P. T., C.-I. Meng, D. G. Sibeck, and R. P. Lepping, Some low-altitude cusp dependencies on the interplanetary magnetic field, *J. Geophys. Res.*, **94,** 8921, 1989.

Reiff, P. H., and J. L. Burch, IMF B_y-dependent plasma flow and Birkeland currents in the dayside magnetosphere. 2. A global model for northward and southward IMF, *J. Geophys. Res.*, **90,** 1595, 1985.

Rich, F. J., and M. Hairston, Large-scale convection patterns observed by DMSP, *J. Geophys. Res.*, **99,** 3827, 1994.

Rodger, A. S., S. W. H. Cowley, M. J. Brown, M. Pinnock, and D. A. Simmons, Dawn-dusk (*y*) component of the interplanetary magnetic field and the local time of the Harang discontinuity, *Planet. Space Sci.*, **32,** 1021–1027, 1984.

Ruohoniemi, J. M., and R. A. Greenwald, Statistical patterns of high-latitude convection obtained from Goose Bay HF radar observations, *J. Geophys. Res.*, **101,** 21 743, 1996.

Tsyganenko, N. A., A magnetospheric magnetic field model with a warped tail current sheet, *Planet. Space Sci.*, **37,** 5, 1989.

Weimer, D. R., Models of the high-latitude electric potentials derived with a least error fit of spherical harmonic coefficients, *J. Geophys. Res.*, **100,** 19 595, 1995.

Wing, S., P. T. Newell, D. G. Sibeck, and K. B. Baker, A large statistical study of the entry of interplanetary magnetic field *y*-component into the magnetosphere, *Geophys. Res. Lett.*, **22,** 2083, 1995.